Molecular Histology of EphrinA1 Expression in Mouse Heart
Visualized with MALDI-MSI

by

Justin Curtis Parks

July 2018

Director of Thesis (Jitka I. Virag)

Major Department: (Biomedical Sciences)

EphrinA1 is a tyrosine kinase receptor localized in the cellular membrane of healthy cardiomyocytes, the expression of which is lost upon myocardial infarction (MI). Intra-cardiac injection of the recombinant form of ephrinA1 (ephrinA1-Fc) at the time of ischemic injury in mice has shown beneficial effects by reducing tissue injury and resultant infarct size post-MI. To date, immunohistochemistry and Western blotting comprise the only experimental approaches utilized to localize and quantify relative changes of ephrinA1 in tissue sections and homogenates of whole left ventricle, respectively. Herein, we used matrix-assisted laser desorption ionization mass spectrometry imaging (MALDI-MSI) coupled with a time-of-flight mass spectrometer (MALDI/TOF MS) to identify intact ephrinA1 in cardiac tissue as well as ephrinA1 fragments that have undergone tryptic digestion. The next step for the characterization and understanding of ephrinA1's role in cardiac tissue was to develop an integrated quantitative method using MALDI-MSI technologies. For this thesis, an optimized a protocol for relative quantitation of endogenous tryptic ephrinA1 peptides detected in the healthy murine myocardium was developed using a standard curve generated with analytical standards. In healthy myocardium, there was approximately 50 ng of endogenous ephrinA1 per tissue section of 9.43 mm^2 average area. MALDI-MSI thus provided a tool for the determination of not only anatomical distribution,

but also relative quantitation of endogenous ephrinA1 in cardiac tissue, advancing our understanding of ephrinA1 expression profile in cardiac tissue. In order to further study ephrinA1 in cardiac tissue, MALDI-MSI was used to study the effects of ephrinA1-Fc treatment 1, 2, 4, and 7 days post-MI. In addition to studying the effects of ephrinA1-Fc on endogenous expression levels of ephrinA1 post-MI, we also inquired about the possibility of gender differences in response to injury as well as EphrinA1-Fc treatment.

Molecular Histology of EphrinA1 Expression in Mouse Heart Visualized with MALDI-MSI

A Thesis

Presented To the Faculty of the Department of Biomedical Sciences East Carolina University

In Partial Fulfillment of the Requirements for the Degree Masters of Science in Biomedical Sciences

By Justin C. Parks

July 2018

Molecular Histology of EphrinA1 Expression in Mouse Heart Visualized with MALDI-MSI

by

Justin Curtis Parks

APPROVED BY:

DIRECTOR OF THESIS: _____

(Jitka I. Virag, Ph.D.)

COMMITTEE MEMBER: _____

(Kimberly A. Kew, Ph.D.)

COMMITTEE MEMBER: _____

(Lisandra E. de Castro Brás, Ph.D.)

COMMITTEE MEMBER: _____

(Tonya N. Zeczycki, P_h.D.)

PROGRAM DIRECTOR MS
IN BIOMEDICAL SCIENCES:_____

(Richard A. Franklin, Ph.D.)

DEAN OF THE
GRADUATE SCHOOL: _____

(Paul J Gemperline, Ph.D.)

Acknowledgments

I would like to thank Dr. Virag for taking me under her wing as an undergraduate student and exposing me to research, with no prior in lab experience, as well as allowing me to stay and complete research with her for my master's, with a measure of freedom and trust. Dr. Virag took a step on a limb to incorporate MSI into her lab, a technique that was new to us all, and I am very thankful and happy she did.

I would like to thank Dr. Kew for introducing me to the world of mass spectrometry and opening the door to a field I would have never pursued without her. Through the entire process of this project she was upbeat and always pushing me to try new ideas, but most of all she was always available to help sort out data or mass spec questions when I was lost.

I would like to thank Dr. Brás for her assistance in data analysis, critical thinking, and problem-solving but most importantly someone who helped me with my writing. Without Dr. Brás my writing would be substantially worse as would be my grasp on some of the more common methods and their troubleshooting steps.

Special thanks to Dr. Zeczycki for her assistance in helping me with Biochemistry and understanding my data and how our protein was behaving. Her assistance in acting as a sounding board and getting me to look at the "bigger picture" was a major contribution to my success as a student.

Finally, my lab mates, without their help this would have been a very difficult and lonely project. Thank you all for keeping me company on those long days, providing laughs while in the lab, and helping me finishing this project.

TABLE OF CONTENTS

LIST OF TABLES

LIST OF FIGURES

LIST OF ABBREVIATIONS

MI: Myocardial infarction

LV: Left ventricle

WT: Wild-type

MALDI-MSI: Matrix assisted laser desorption ionization mass spectrometry imaging SA: Sinapinic acid

CHCA: α-cyano-4-hydroxycinnamic acid

DHB: 2, 5-Dihydroxybenzoic acid

RMS: Root mean square

TIC: Total ion current

MALDI/TOF MS: Time-of-flight mass spectrometer

Eph-R: Ephrin family receptors

EA1-Fc: EphrinA1-Fc

1D: 1-day

2D: 2-day

4D: 4-day 7

D: 7-day

CHAPTER ONE: INTRODUCTION

Heart disease is currently the most significant cause of morbidity and mortality in the United States, with almost 800,000 people affected and killing nearly 14.5% of heart attack victims annually. In addition to the risk to their life, the financial burden is overwhelming. In 2017, heart attacks were among most expensive hospital diagnoses. It is estimated that the costs associated with heart attacks will continue to increase up to 100% by 2030 (Benjamin et al. 2017). The combination of mortality rates and rising costs means there is a desperate need for the development of a therapeutic method. Currently, reperfusion therapy is the gold standard of care for those patients that experience an ischemic event, however there are some limitations and pitfalls with this treatment method. In order for reperfusion to be effective it must be applied within hours of the injury and even then, patients still have the possibility of worsening the oxidative injury with reperfusion (Michael et al. 1999, Jones et al. 201, Vandervelde et al. 2006). At this point in time there is still a lack of cardio-protectants that reduce infarct size in patients.

The Eph-R-Ephrin family is the largest family of receptor tyrosine kinases. EphrinA1 is a membrane-bound receptor tyrosine kinase that is expressed in healthy cardiomyocytes. It is the only member of the ephrinA family that can bind to all eight of the EphA-R expressed in mice (Easty et al. 1999). The Eph-R- Ephrin family are responsible for cellular functions such as cell differentiation, proliferation, migration during development (Pasquale 2008, Easty et al. 1999) and tumorigenesis (Brantley et al. 2002, Dodelet and Pasquale 2000, Brantley-Sieders et al. 2004, Surawska, Ma, and Salgia 2004). An intramyocardial administration of chimeric ephrinA1-Fc in mice at the time of injury attenuates damage post-MI (Pasquale 2008, Pandey et al. 1995, Cheng, Brantley, and Chen 2002, Dries, Kent, and Virag 2011, A. DuSablon et al. 2014, A. DuSablon et

al. 2017, O'Neal et al. 2013, O'Neal et al. 2014, Coulthard et al. 2012). Specifically, ephrinA1-Fc injected intramyocardially at time of MI reduces damage to the tissue independent of changes in vascularity. This reduction of injury results in a reduction of infarct size of up to 50% and necrosis by 64%, chamber dilation by 35%, and free wall thinning by 32% in the left ventricle four days post-MI. Preservation of functional myocardial tissue translates to retention of cardiac function as compared to those that do not receive the treatment. (Dries, Kent, and Virag 2011).

Gaps in the widely practiced biological tests such as IHC and Western blotting are resulting in missed opportunities to gain a deeper understanding of the problems at hand such as quantitative as well as qualitative data. Conventional biological experimental tools do not provide both quantitative and qualitative data during the same experiment. Although these techniques are valuable and do provide much needed data, it is time to use these tools in conjunction with newer and more powerful techniques. The more common methods of obtaining the spatial distribution of protein expression in tissue sections were confined to immunohistochemistry (IHC). IHC is a technique that can be quite restrictive regarding the number of targets that are identified in a section by the antibody specificity, subcellular localization of the antigen, and color compatibility of the chromogen/fluorescent labels (Cornett et al. 2007). Specifically, IHC can be challenging to identify co-localizing targets as color detection can mix and become difficult to determine. In addition to this, there is a limitation as to the color options available to use, reducing the total number of targets in each sample. Immunohistochemistry is a valuable and widely-used tool to look at expression distribution changes in samples, yet it does not have the power to address protein expression levels. Furthermore, fluorescent IHC is susceptible to photo-bleaching, in which exposure to light reduces the fluorescent signal. The use of antibodies in IHC increase the complexity of the analysis while also generating a gap in the analysis and requires a number of

components that must be optimized. Even with this optimization, the potential for non- specific binding is an ever-present concern. In addition to IHC, immunoblotting is used as a tool for relative quantitation using standard curves, however this is limited in that only pure standards can be used in this curve. Also immunoblotting requires the use of antibodies which, if available, are costly and can have possible non-specific. Unlike IHC and immunoblotting, MALDI-MSI can detect multiple targets simultaneously potentially generating expression profiles for multiple targets of interest. While MALDI-MSI can target multiple targets simultaneously it also eliminates the possibility of photo-bleaching as well as non-specific binding.

MALDI-MSI was first used in the late 1990's to spatially map the location of proteins of interest in intact tissue (Caprioli, Farmer, and Gile 1997). Following spatial mapping of intact tissue in 2007, it was found that proteins could be identified directly from tissue using *in situ* trypsin digestions in conjunction with imaging mass spectrometry (Wagner et al. 2007). When MALDI was coupled with a time-of-flight mass spectrometer (MALDI/TOF MS), a broad mass range could be covered and provided the opportunity to detect intact protein as well as protein that had undergone enzymatic digestion (Liu and Schey 2005). MALDI-MSI is a versatile tool that is used in the identification of metabolites, lipids, peptides, and proteins directly from tissue sections while providing a much higher spatial resolution than can be obtained from IHC methods (Liu and Schey 2005, Caprioli, Farmer, and Gile 1997).

Qualitative MALDI-MSI technologies have provided an attractive approach for the characterization of the spatial distribution of proteins in tissue sections, previously limited to histology and immunohistochemistry. MALDI-MSI provides a powerful quantitative tool to detect multiple proteins in a single tissue section. Furthermore, MSI data sets may be reanalyzed in the future for any number of possible variations within each data set. Some quantitative analyses have

been done for the study of functional organ anatomy of the adult human adrenal gland using metabolite (Sun et al. 2018). In addition to these studies quantitative analyses have been completed targeting drug compounds, biological fluids and extracts, and exogenous compounds in biological systems such as drugs compounds, growth hormone or antibiotics but there is limited work using MALDI- MSI to conduct relative protein quantitation. (Chumbley et al. 2016, Reich et al. 2010, Bucknall, Fung, and Duncan 2002)

MALDI-MSI has been used for quantifying exogenous compounds, such as cocaine, methadone and naltrexone, and Rifampicin in brain and liver tissues in order to track where the exogenous compounds are located (Reich et al. 2010), (Teklezgi et al. 2018, Chumbley et al. 2016). In addition to exogeneous compounds, MALDI-MSI has been used to study protein and peptide distribution. Relative protein quantitation has been reported with MALDI-MSI using either isotope labeling such as ^{2}D, ^{13}C, ^{15}N, or ^{18}O labeling; a chemical tag (i.e. p-hydroxymercuribenzoic acid) (Kutscher and Bettmer 2009); or label-free relative quantitation (Albalat et al. 2013). Examples of relative quantitative protein analysis from the literature include myelin proteolipid protein in brain tissue samples using MALDI-MSI and LC/MS as conformation (Nicklay et al. 2013); and MALD multiple reaction monitoring imaging for labeled myelin basic protein in rat brain tissues (Clemis et al. 2012). From the literature, there is a gap focusing on the use of biological samples and determining relative quantitation of endogenous proteins specifically those undergoing trypsin digestion. It is the goal of this projects to show MALDI-MSI is a robust and accurate to gain relative quantitative values of ephrinA1 in healthy murine cardiac tissue based on comparing response levels from a recombinant ephrinA1-His tag standard. This not only lead to a higher understanding of endogenous protein levels it also provided an opportunity to grasp the effects exogenous treatment of ephrinA1-Fc on cardiac tissue over various time points post-MI and the

effects it has as a therapeutic.

CHAPTER TWO: METHODS

Animal use –

Experimental research protocols were approved by the East Carolina University Institutional Animal Care and Use Committee (IACUC) following the guidelines of the National Institutes of Health for the Care and Use of Laboratory Animals. Animal care was maintained by the Department of Comparative Medicine at The Brody School of Medicine, East Carolina University. B6129SF2/J (stock #101045) 8-12-week-old wild-type (WT) male mice and female were purchased from the Jackson Laboratories. Mice were housed with 12 hr/12 hr light/dark cycle conditions and were fed and given water ad libitum. Animals were anesthetized with euthasol (100 mg/Kg BW) and sacrificed for tissue collection.

Surgical procedure –

Mice were anesthetized with an intraperitoneal injection of Avertin (20 mg/Kg body weight, BW) and mechanically ventilated with 95% O2/5% CO2 which is used to supplement air supply found in surgery room. A thoracotomy was performed, and myocardial infarction was induced by occluding the LAD using an 8-0 suture. Ischemia was confirmed by visible blanching of the tissue distal to the occlusion. The rib cage, muscle, and skin were closed sequentially, and the animals were allowed to recover over a heating pad. Post-MI animals were anesthetized with euthasol (100 mg/Kg BW) and sacrificed for tissue harvest. Whole hearts were thoroughly perfused with ice-cold PBS (10– 15 mL, for 2–3 min), wrapped loosely in foil, and snap-frozen in liquid nitrogen. Samples were then stored at –80 °C.

Cryosectioning –

Frozen tissues were mounted on a cryostat chuck with water and allowed to freeze at -80 ˚C for 5 min. 10 µm thick sections resulting in an average area of 9.425 mm2 were then thaw-mounted on an Indium tin oxide (ITO) coated glass slide. Slides were washed for 30 sec sequentially in 70 %, 90 %, and 95 % ethanol, and then placed in a vacuum desiccator with Drierite for 30 min (Yang and Caprioli 2011). EphrinA1- His tag standards were added as described below for relative quantitation.

Analytical standards –

EphrinA1-His tag standards were diluted in water prior to use. Concentrations of 10, 25, 50, and 100 µg/mL ephrinA1-His tag standards were used for optimization (matrix selection and tryptic digestion time) and confirmed prior to dilution by BCA assay. For relative quantitation of endogenous ephrinA1 in tissue, concentrations of 10, 35, and 50 µg/mL of the ephrinA1-His tag standard were used. In all cases, 1 µL of the standard was pipetted directly onto ITO slides, and allowed to dry in an incubator at 37 ˚C. Slides were incubated for a duration of 1, 2, 4, 6 and 8 hrs. At each time point, four different trypsin concentrations 10, 20, 40, or 100 µg/mL were utilized to determine the optimal digestion concentration for ephrinA1.

Optimization of matrix deposition–

For method development and optimization, three methods for matrix deposition were tested utilizing standards and control tissue for intact protein analysis: (1) direct delivery, (2) thin layer

chromatography (TLC) sprayer (Sigma-Aldrich, Z529710, 10 mL), and (3) TM sprayer (HTX Imaging). (1) For the first experiment, 0.5 µL of the sinapinic acid (SA) matrix was applied using a micropipette in multiple regions across the control tissue for intact ephrinA1 signal optimization and mixed 1:1 with the analytical standard next to the tissue for mass calibration and verification. (2) A TLC sprayer was manually used to apply SA matrix, and the standard was applied near the tissue after matrix deposition. N2 was used at a low flow rate (< 5 psi), and psi was optimized based on the spray distribution. Two spray passes were performed before allowing the slides to completely dry. This process was repeated to add and build layers of a matrix using a total of 20 mL of the matrix. (3) A TM sprayer was used to apply SA matrix under the following conditions: 0.1 mL/min solvent flow rate, 10 psi N2 gas pressure, 30 °C nozzle temperature, 750 mm/min velocity, spacing of 2 mm, and four passes over the entire slide.

Matrix selection–

Three matrices were tested for optimal detection of ephrinA1 standard: 2′,6′-Dihydroxyacetophenone (DHA), α-cyano-4-hydroxycinnamic acid (CHCA), and SA. All matrices were tested at 10 mg/mL in 70:30 acetonitrile: water with 0.3% Trifluoroacetic acid (TFA) 60:40 acetonitrile: water with 0.1% TFA, and 70:30 acetonitrile: water with 0.1% TFA. The ephrinA1 standard was spotted with matrix 1:1 on a target plate and the intact protein signal was used to optimize the MALDI instrument parameters in positive ionization mode.

Intact ephrinA1 MSI –

Imaging experiments were performed using a Bruker Autoflex Speed MALDI/TOF-TOF mass spectrometer. Before matrix deposition, tissues were scanned using an Epson flatbed scanner and collected

at 300 dpi for the acquisition of a digital baseline image. The mass spectrometer method was set to collect 5000 spectra/spot and images. Intact protein images were collected using linear mode, and trypsin peptide images were collected using reflectron mode. Calibration was conducted using a mixture of angiotensin II, bovine insulin, PEG 600, and ephrinA1-His standard. All control and acute MI samples were imaged at 100 µm spatial resolution. Data were collected in positive ionization mode and a Nd:YAG laser repetition rate of 2000 Hz was used (50 µm laser size) during image collection.

Trypsin solution –

A stock solution was made using 20 µg of trypsin which was resuspended in a total of 440 µL containtng 50 mM acetic acid (resuspention solution), ammonium bicarbonate containing 0.01 % ammonium hydroxide, acetonitrile, and 100 mM acetic acid resulting in final a concentration of 40 µg/mL. Slides were incubated in and incubator at 30˚ C for 30 minutes to ensure enzyme activation.

Tissue trypsin digestion –

Tryptic digestion of tissues was performed with the same trypsin solution, activation time, and temperature. Trypsin addition was completed using the HTX TM sprayer and a syringe pump. Parameters were as described previously set at a flow rate of 60 µL/min, for 2 passes at 600 mm/min, track spacing of 2 mm with a crisscross pattern at 12 psi, a nozzle height of 40 mm and a 3 l/min gas flow rate.

In-solution protein digestion –

In-solution trypsin digestions were performed using the UAB proteomics method (Mobley, J. 2008). Briefly, non-denatured samples were exposed to 200 mM DTT/50 mM Tris HCl followed by 200 mM iodoacetamide/50 mM Tris HCl in the dark. DTT/Tris HCl was added one more time to consume any un-reacted iodoacetamide. The same trypsin solution used for ephrinA1-His tag standards and tissue was added at a ratio of 1:50 (trypsin/protein) and incubated at 37 ˚C for 18 hrs. The same experimental procedure was followed for denatured samples, but with boiling for 5 minutes at 95 ˚C prior to the DTT/Tris-HCl incubation.

Trypsin digested sample matrix application –

The matrix consisted of 10 mg/mL CHCA or SA in 70:30 acetonitrile: water 0.3 % TFA. During method optimization (matrix selection and trypsin digestion), either CHCA or SA was pipetted (1 µL) on top of the analytical standard and allowed to dry at room temperature. The matrix was added to ITO slides using the HTX TM Sprayer (HTX Technologies LLC, Chapel Hill, NC), with parameters set at 30 ˚C for 12 passes with a flow rate of 0.1 mL/min at 750 mm/min. Track spacing was set at 2 mm using a crisscross pattern at 10 psi with a gas flow rate of 0.1 mL/min and nozzle height of 40 mm. In- solution digestion experiments used SA matrix that was pipetted (1 µL) and allowed to dry before sample addition. After the sample was added to the plate, it was allowed to dry, and another µL of the matrix was pipetted on top of the sample.

Trypsin digested sample MALDI settings –

Prior to trypsin digestion, ephrinA1-His tag standards at concentrations of 0.001, 0.1, 1,10,

35, 50, and 100 µg/mL were pipetted onto the slide and allowed to dry. Dry slides were scanned at 2400 dpi with teach markings for spatial orientation placed at the corners and loaded into FlexImaging for determination of regions of interest. All experiments were completed using reflectron positive mode with laser power optimized for signal intensity (104) with a mass range of 0 to 5000 *m/z*. During method optimization, 5000 spectra were collected per sample at a frequency of 2000 Hz. For in-solution digestion experiments, 8000 spectra were collected for each sample, and for relative quantitation of endogenous ephrinA1, 8000 spectra were collected per laser shot with spectra collected every 75 µm. FlexImaging was used to collect the data along with FlexControl and FlexAnalysis for spectra.

Trypsin digested sample data analysis –

The sequence of ephrinA1-His tag was theoretically digested using the protein prospector databasehttp://prospector.ucsf.edu/ based on the amino acid sequence and predicted cleavage sites. Parameters included digestion by trypsin with a max of 5 possible missed cleavages, no variable modifications, a peptide mass range of 400-5000 *m/z*, a minimum peptide length of 5, and MALDI-TOF-TOF instrumentation to provide *m/z* values and predicted sequences from ephrinA1 tag standards. Protein prospector theoretical *m/z* data was compiled and compared to experimental *m/z* values found. Spectra generated to determine optimal matrix and digestion time were analyzed with flexanalysis, calibrated using PEG 600 and angiotensin II, and normalized to total ion current. Spectra were processed using centroid algorithm with a signal-to-noise ratio of 3. Peak width was set at 2 *m/z* and height 10%. All spectra were smoothed once with single baseline subtraction using TopHat algorithm and were smoothed once using SavitzkyGolay with a width of 0.2 *m/z* at 1 cycle.

Cartoon modeling of EphrinA1 and image analysis –

EphrinA1 cartoon structure was generated based on the PDB file 3CZU (Himanen et al. 2010) using PyMOL (v 1.8, Schordinger LLC). Mass lists were compiled using SCiLS software from imaged healthy control cardiac tissue and ephrinA1-His tag standards. Spectra in SCiLS Lab were aligned to the mean spectra, then exported as overview spectra in CSV file with an intensity threshold of 6. Protein prospector's MS-Bridge feature and mass lists generated from SCiLS lab, sequences found in each sample were identified and matched to sequences found in the in-solution data. For relative quantitation of ephrinA1 in cardiac tissue, MALDI-MSI data was imported to SCiLS Lab software and known ephrinA1 *m/z* peaks were selected. Using known ephrinA1 *m/z* intensity box plots, reconstructed ion images were created to match tryptic peptides from the ephrinA1-His tag standard and endogenous ephrinA1. Reconstructed ion images intensities were adjusted for each *m/z* to visualize ephrinA1 and ephrinA1-His tag standards.

Data analysis –

The sequence of ephrinA1-His tag was theoretically digested using the protein prospector database (http:// prospector.ucsf.edu/) based on the amino acid sequence and predicted cleavage sites. Parameters included digestion by trypsin with a max of 5 possible missed cleavages, no variable modifications, a peptide mass range of 400-5000 *m/z*, a minimum peptide length of 5, and MALDI-TOF-TOF instrumentation to provide *m/z* values and predicted sequences from ephrinA1 tag standards. Protein prospector theoretical *m/z* data was compiled and compared to experimental *m/z* values found. Spectra generated to determine optimal matrix and digestion time were analyzed with flexanalysis, calibrated using PEG 600 and angiotensin II, and normalized by total ion current. Spectra were processed using centroid algorithm with a signal to noise ratio of 3. Peak width was set at 2 *m/z* and height 10 %. All spectra were smoothed once with single baseline subtraction.

Echocardiography –

Echocardiography was performed blindly at mid-papillary level (evidenced by the presence of brush strokes at systole) on conscious, restrained mice at 24hrs or 4 days post-MI. A VisualSonics Vevo 2100 diagnostic ultrasound, using M-mode and 30MHz probe, was used to obtain LV dimensions in diastole and systole using standard procedures and calculations as previously described (Yang et al, 1999, DuSablon et al, 2014)

CHAPTER 3: Anatomical-Molecular Distribution of EphrinA1 in Infarcted Mouse Heart Using MALDI Mass Spectrometry Imaging

INTRODUCTION

EphrinA1 is a tyrosine kinase receptor localized in the cellular membrane of healthy cardiomyocytes, the expression of which is lost upon myocardial infarction (MI). Intra-cardiac injection of the recombinant form of ephrinA1 (ephrinA1-Fc) at the time of ligation in mice has shown beneficial effects by reducing infarct size and myocardial necrosis post-MI. To date, immunohistochemistry and Western blotting comprise the only experimental approaches utilized to localize and quantify relative changes of ephrinA1 in sections and homogenates of whole left ventricle, respectively. Herein, we used matrix-assisted laser desorption ionization mass spectrometry imaging (MALDI-MSI) coupled with a time-of-flight mass spectrometer (MALDI/TOF MS) to identify intact as well as tryptic fragments of ephrinA1 in healthy controls and acutely infarcted murine hearts. The purpose of the present study was 3-fold: (1) to spatially resolve the molecular distribution of endogenous ephrinA1, (2) to determine the anatomical expression profile of endogenous ephrinA1 after acute MI, and (3) to identify molecular targets of ephrinA1-Fc action post-MI. The tryptic fragments detected were identified as the ephrinA1-isoform with 38% and 34% sequence coverage and Mascot scores of 25 for the control and MI hearts, respectively. By using MALDI-MSI, we have been able to simultaneously measure the distribution and spatial localization of ephrinA1, as well as additional cardiac proteins, thus offering valuable information for the elucidation of molecular partners, mediators, and targets of ephrinA1 action in cardiac muscle

RESULTS & DISCUSSION

Matrix selection and Intact ephrinA1 MSI –

Comparison of several MALDI matrices DHA, CHCA, and SA revealed SA to be the optimal matrix for detection of the intact ephrinA1 recombinant protein. Using positive ionization linear detection, doubly charged, protonated, and dimer forms were identified in the mass spectra (Fig. 1).

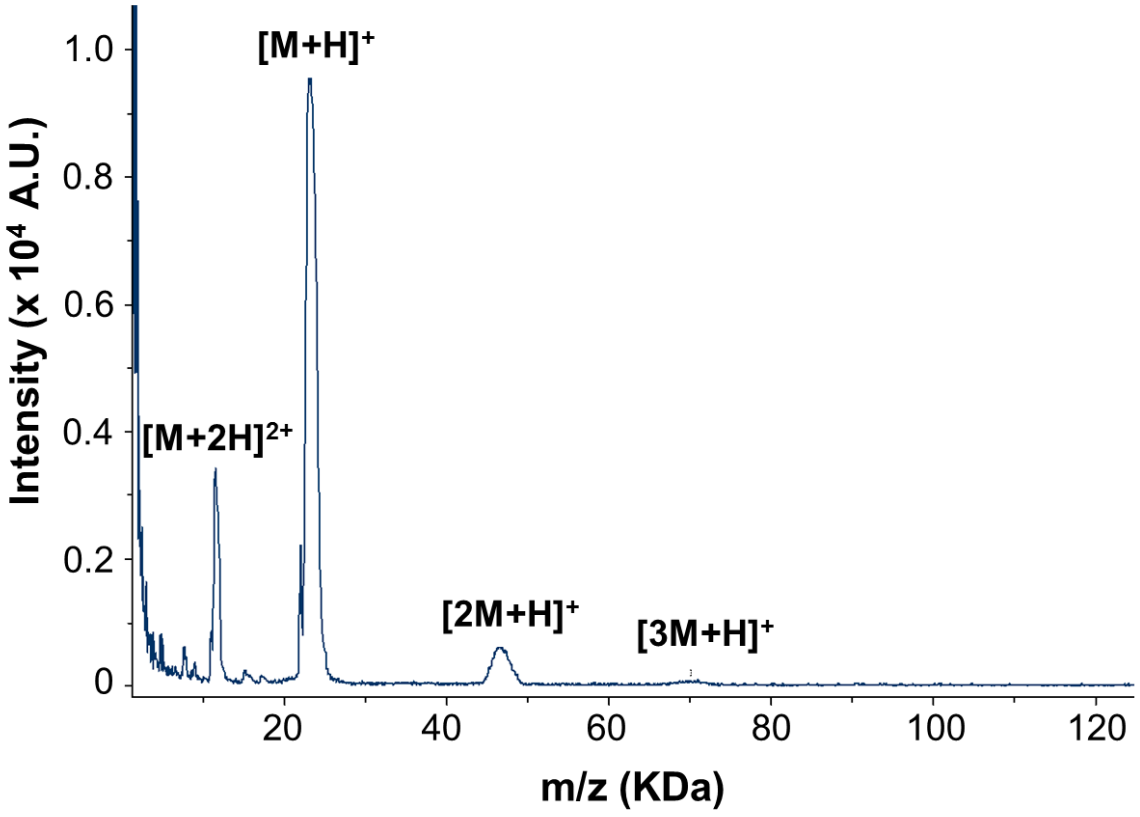

Figure 1: Mass Spectra for EphrinA-His tag Standard. Representative mass spectra for ephrinA1-His standard for the analysis of the intact protein.

To validate the selectivity of the standard, the sequence reported by the manufacturer was blasted against all databases using the National Center for Biotechnology Information (NCBI, US National Library of Medicine). EphrinA1 (His tag) was found to have a 349-maximum score, 94% query coverage, and a 100% identification for ephrinA1 isoform 1 precursor [Mus musculus]. Washing has been found to significantly increase protein detection limits by reducing the suppression of ionization normally caused by lipids and small molecules. Previously reported methods were modified (Aichler and Walch 2015, Seeley, Schwamborn, and Caprioli 2011) to include sequential ethanol washes after the tissue sections were fixed to the ITO slides, and this significantly improved the detection of ephrinA1. Three different methods of matrix deposition were compared: direct delivery, TLC sprayer, and TM sprayer. The reconstructed chemical ion image for intact ephrinA1, as well as the respective mass spectra for each method, is shown in Figure 2. Intact protein signals were best detected with direct delivery and utilization of the TM sprayer. Although ephrinA1 was detected with all three matrix applications, the samples prepared using the automatic TM sprayer for matrix deposition provided the most uniform reproducible signal distributions across the tissue (Figure 2c) attributable to the mechanism of the nozzle and the nature of the deposition of matrix.

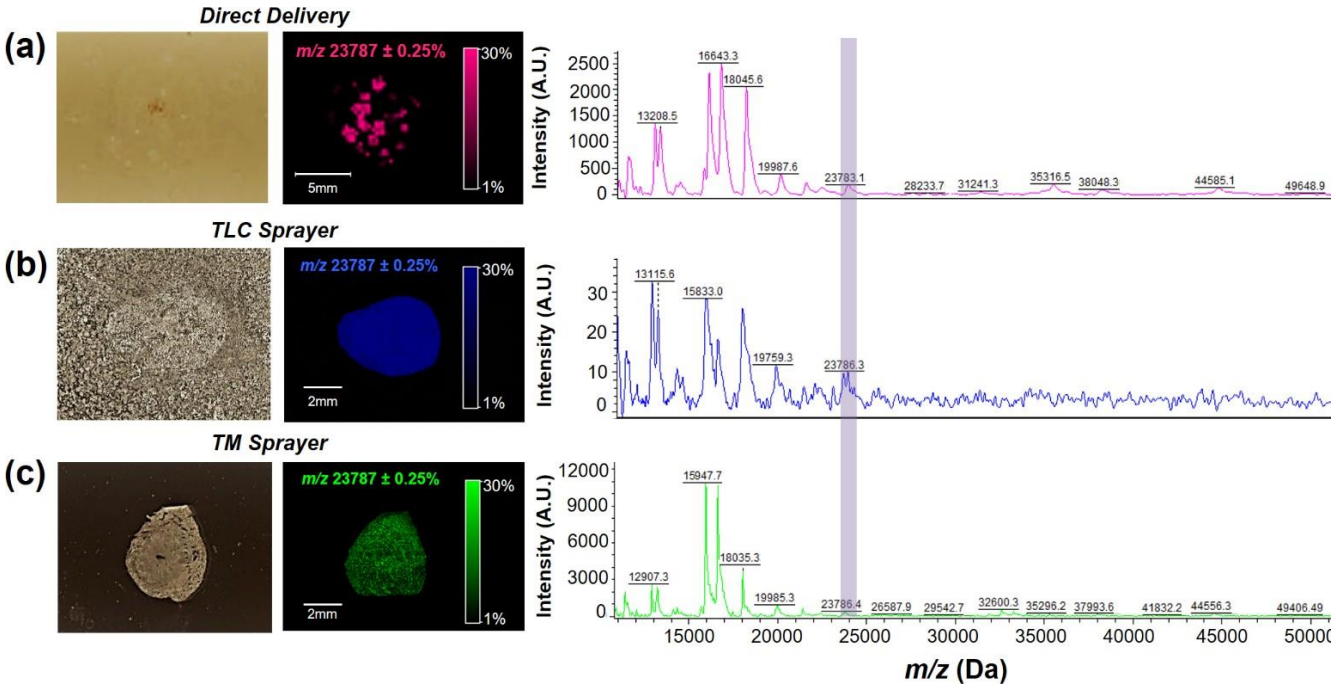

Figure 2. Reconstructed Chemical Images of Intact EphrinA1 in Healthy Heart Tissue Using 3 Different Matrix Deposition Techniques. Representative pictures of chemical reconstruction images for a healthy heart using three different matrix deposition techniques: (a) direct delivery at *m/z* = 23783.1 (S/N 189), (b) TLC prayer at *m/z* 23786.3 (S/N 10), or (c) TM sprayer at *m/z* = 23786.4 (S/N 97). The purple bar highlights the peak at 23.7 kDa, which represents the intact molecular ion for ephrinA1

Method Validation for Imaging of Cardiac Tissue –

The molecular distribution of creatine was investigated for method validation in cardiac tissue. Creatine, which serves as a rapid energy source in cardiac tissue via the creatine/ phospho-creatine system, is abundant in healthy cardiac tissue, but found to be drastically reduced in infarcted ischemic tissue (Menger et al. 2012). The molecular ion of creatine (*m/z* = 132 Da) yields a primary fragment of *m/z* = 90 Da. Creatine and its primary fragment are shown in Figure 3, as detected in a section from a healthy control (a) and post-MI heart (b). The primary fragment of creatine presented lower signal intensity in the ischemic region post-MI. These findings are in

agreement with previous reports correlating lower creatine levels with regions of necrosis, and particularly upon persisting ischemia [(Menger et al. 2012). Overall, the data support MALDI-MSI as a valid method to image murine cardiac tissue and elucidate molecular signatures post- MI.

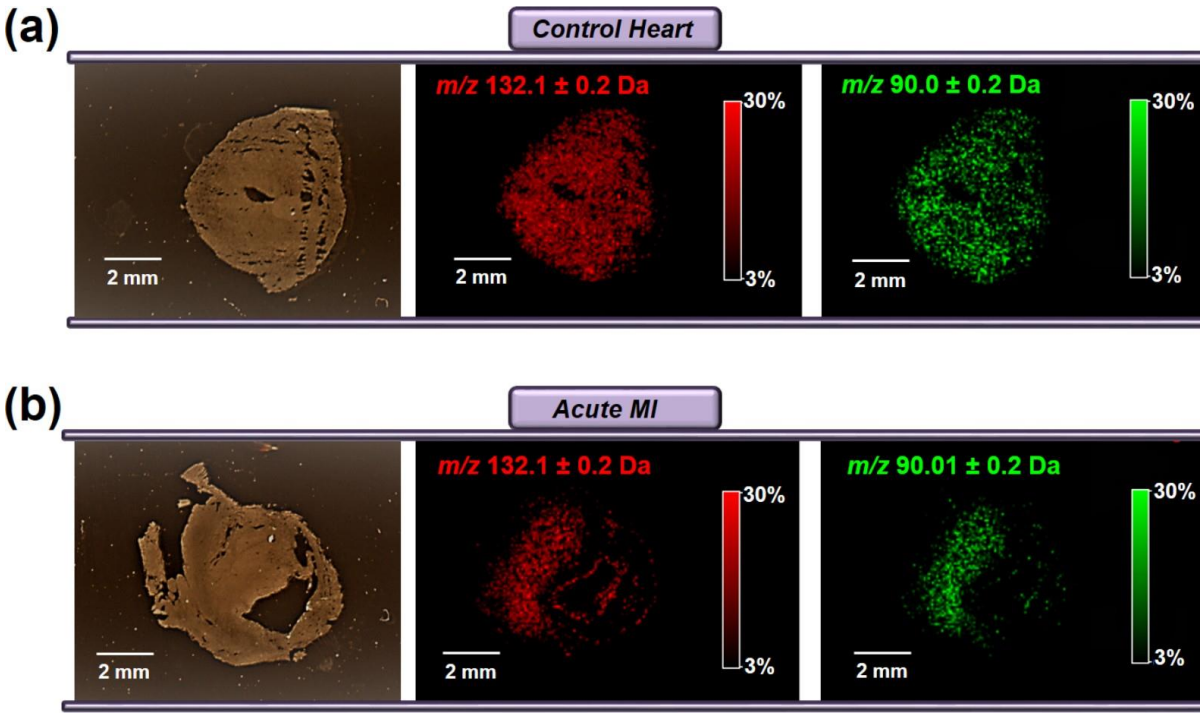

Figure 3. Spatial distribution of creatine (*m/z* = 132 Da, shown in red) in healthy control (a), and post-MI (b) murine hearts. When creatine is subjected to MS/MS analysis, a primary fragment is observed at *m/z* = 90 Da, corresponding to the protonated ([M + H] +) n-methylglycine (shown in green)

EphrinA1 Expression Profile in Murine Heart –

To determine ephrinA1 spatial distribution, heart sections were subjected to trypsin digestion. A 4-hour incubation provided the highest number of identified tryptic fragments and sequence coverage. EphrinA1-His tag standard was also spiked in healthy control hearts prior to

trypsin digestion as an analytical control, and the observed peptides were confirmed. A representative average mass spectrum is shown in Figure 4. Mascot scores for ephrinA1 were 41, 25, and 25 for the standard, spiked tissue, and tissue, respectively. The Mascot score was low for the standard due to the nature of the analysis, the primary limiting factor being sample preparation for protein analysis in tissue on a surface (proteins are not fully denatured and only partially trypsinized). Taking this into consideration, the standard was treated consistently with tissue samples.

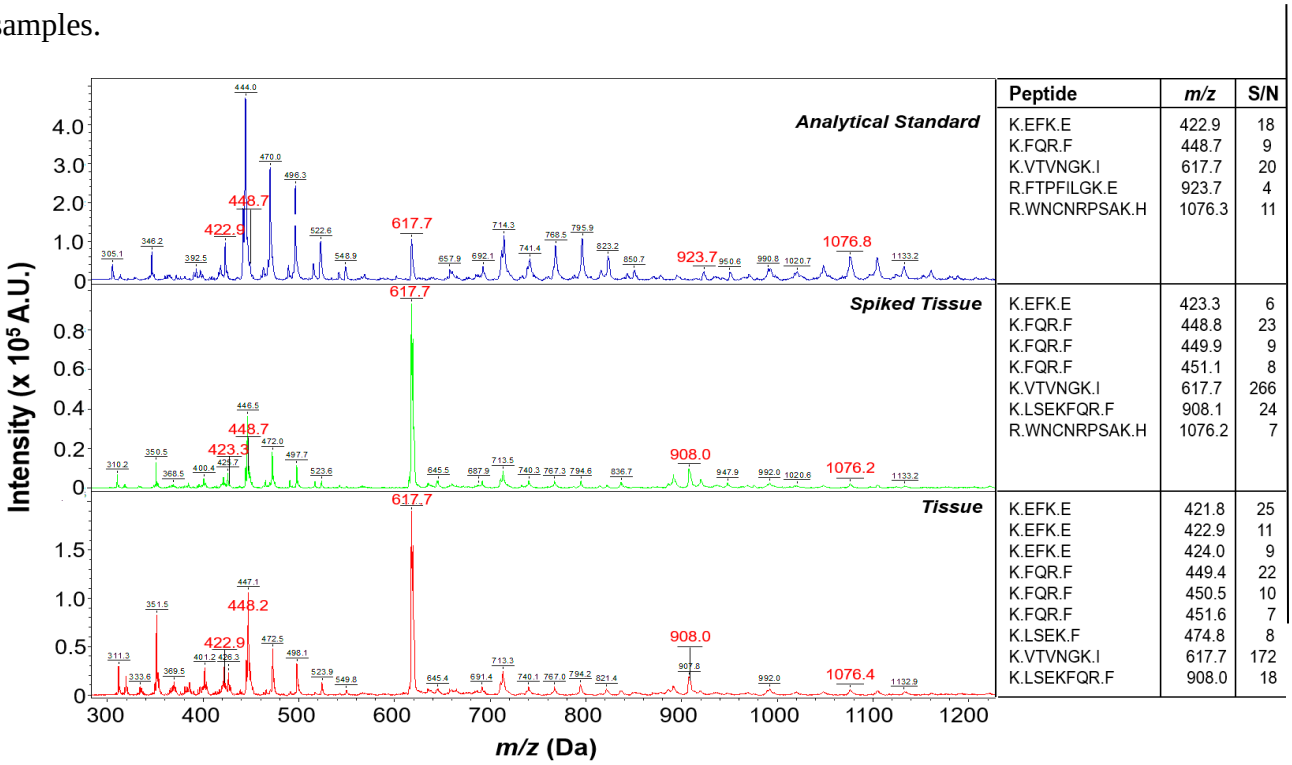

Peptide	m/z	S/N
K.EFK.E	422.9	18
K.FQR.F	448.7	9
K.VTVNGK.I	617.7	20
R.FTPFILGK.E	923.7	4
R.WNCNRPSAK.H	1076.3	11
K.EFK.E	423.3	6
K.FQR.F	448.8	23
K.FQR.F	449.9	9
K.FQR.F	451.1	8
K.VTVNGK.I	617.7	266
K.LSEKFQR.F	908.1	24
R.WNCNRPSAK.H	1076.2	7
K.EFK.E	421.8	25
K.EFK.E	422.9	11
K.EFK.E	424.0	9
K.FQR.F	449.4	22
K.FQR.F	450.5	10
K.FQR.F	451.6	7
K.LSEK.F	474.8	8
K.VTVNGK.I	617.7	172
K.LSEKFQR.F	908.0	18

Figure 4. Mass spectra from ephrinA1 analytical standard (top panel), control tissue spiked with standard (middle panel), and healthy control tissue (bottom panel)

The ephrinA1 sequence is listed in Figure 5a. The detected tryptic peptides and reconstructed chemical images for selected ephrinA1 ions detected in control and MI hearts are shown in Figure 5b (top and bottom, respectively). Healthy control hearts matched with 14 out of the 25 predicted

weights yielding a 38% coverage, whereas the MI hearts only matched seven out of the 25 masses, yielding a 34% coverage. There were five additional peptide fragments detected in the healthy tissue that were not detected in either the standard or the MI. The reduction in the number of peptides in the MI samples is attributed to the lower abundance of ephrinA1 post-MI, in agreement with previous immunohistochemical and Western blot reports (O'Neal et al. 2014).

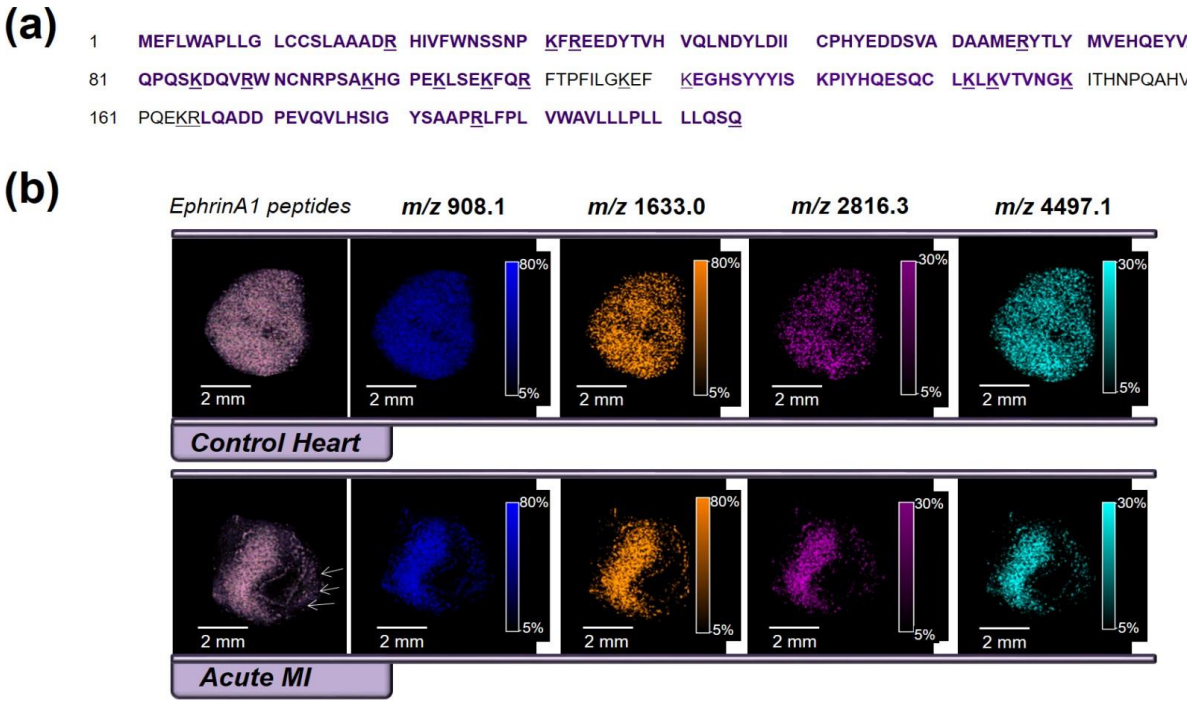

Figure 5. EphrinA1 in the heart. (a) The primary sequence of ephrinA1 with trypsin cleavage sites enoted by underlined lysine (K) or arginine (R) amino acids. Murine sequence NCBI accession NP_034237, generated using the MS-Bridge program athttp://prospector.ucsf.edu/ allowing for one missed cleavage. (b) Expression profile of trypsinized ephrinA1 fragments: matches between theoretical and detected fragments from a control, healthy heart (top), and after acute MI (bottom) are shown. Selected ephrinA1 trypsin fragments that are present in a control healthy heart (m/z = 908, 1632.96, 2816.25, and 4497.11 Da) but not in the region at risk from the infarcted heart are shown

The experiment was repeated in n = 6 healthy control hearts and n = 6 MI hearts. EphrinA1

matching masses presented average protein prospector scores of 73 ± 17% and 42 ± 39% for the healthy and MI samples, respectively. There were 25 peptides specific for ephrinA1, detected with a S/N ≥ 3, and the frequency of detection per the sample is shown in Figure 6.

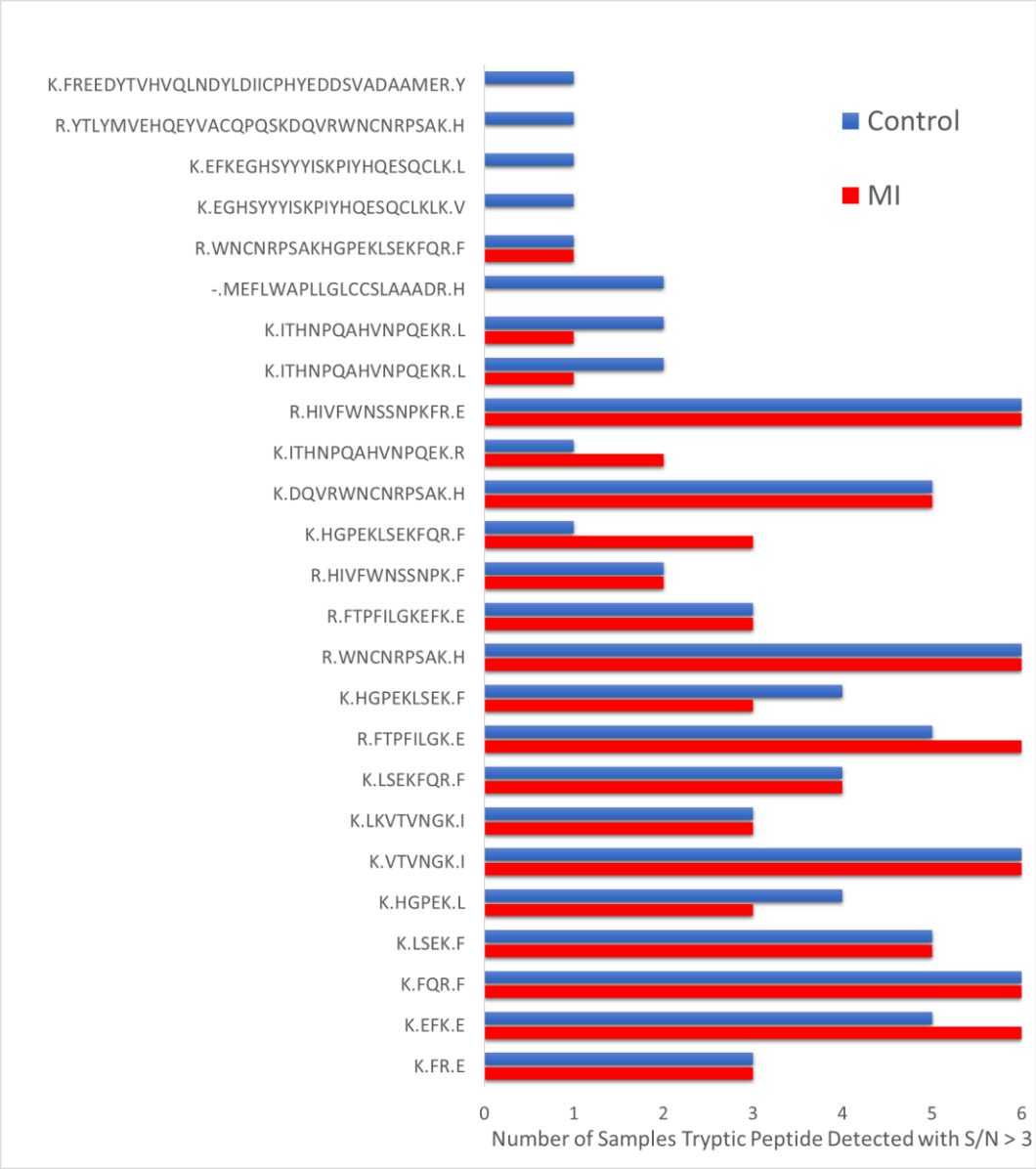

Figure 6: Frequency distribution for tryptic peptide detection in healthy and MI heart tissues with n=6 per group.

Target Cardiac Proteins Post-MI –

Further analysis was conducted in post-MI tissue comparing proteins across specified regions. Three mass spectra were extracted from each defined region across the injured tissue and a Mascot search was conducted to obtain tentative protein identification. Selected regions across the infarcted heart included the remote (in the same plane as the injury but not affected by the ligation), border (the intersection of injured tissue with uninjured tissue), and injured areas are shown in the H&E stain (Figure 7a). A reconstructed chemical ion image for m/z 617.2 shows the expression profile of ephrinA1, which was used to define the regions for MALDI-MSI extraction (Figure 7b). The Venn diagram in Figure 7c shows the overlap among the number of proteins identified within the three defined regions. Table 1 shows the top tentative protein identifications in healthy control versus post-MI regions of interest (remote, border, and infarct) obtained from a 4-hr trypsin digest. Additional protein identification was achieved by sequence matching against Mascot, although this was not further validated with a secondary technique. The proteins depicted in table 1 warrant further investigation to elucidate the role of endogenous ephrinA1 in the cardiomyocyte, as well as its molecular targets upon acute MI. Specifically, pathways involved in mitochondrial energetics and autophagic flux are of great interest to understand the molecular mechanisms by which ephrinA1-Fc mediates preservation of myocardial tissue integrity and cardiac function upon MI.

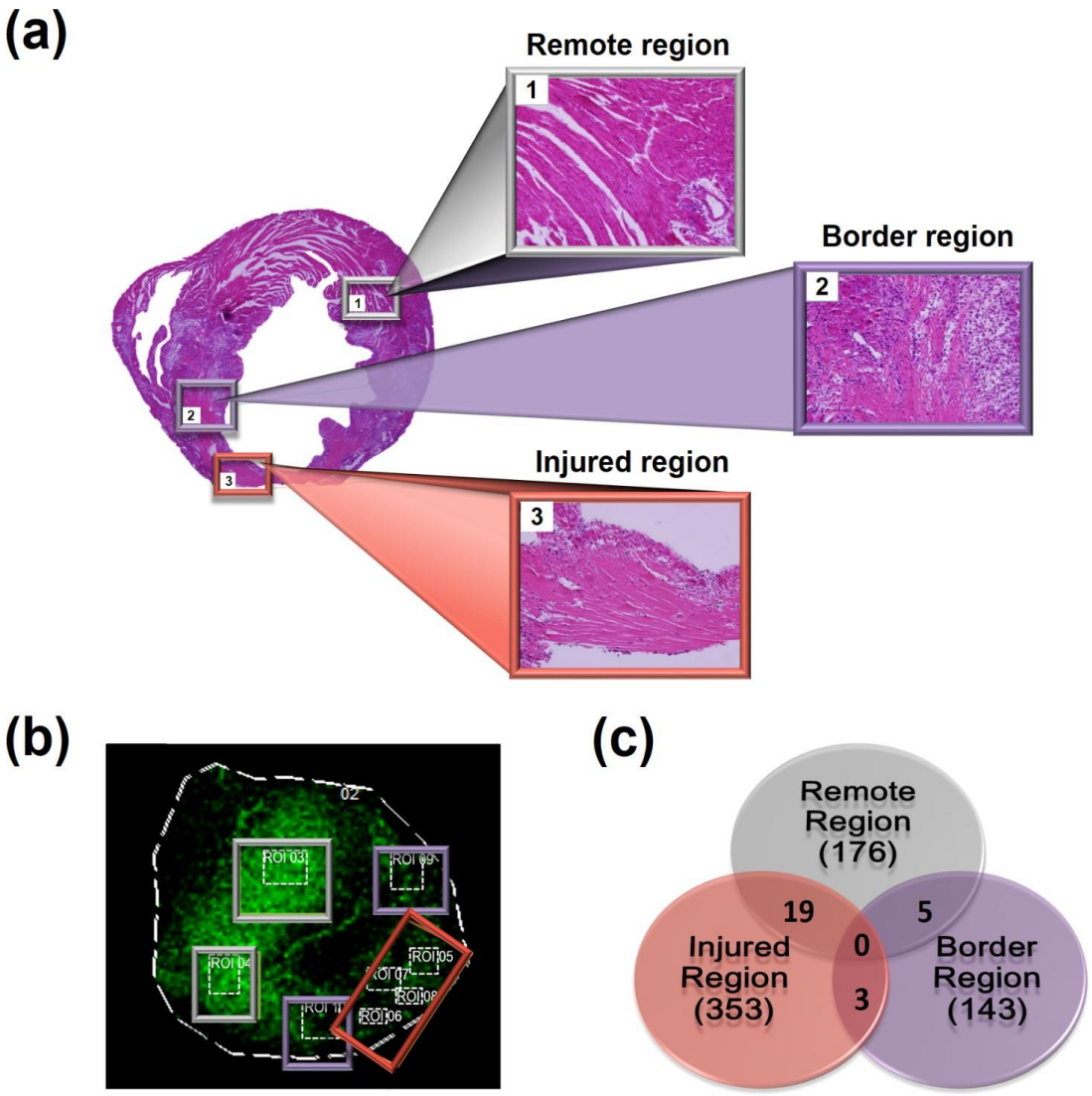

Figure 7. Regions of interest selected for tentative global protein identification post-MI. (a) Histological images (H&E) defining the remote (1), border (2), and infarcted (3) regions. (b) Reconstructed chemical image using *m/z* = 617.2 Da and selected regions of interest for extracting mass spectra for Mascot database searching. (c) Diagram showing total numbers of tentatively identified proteins per region and overlapping proteins

The functional annotation tool (DAVID 6.8) was used to identify 18, 30, 21, and 61 clusters the healthy remote, border, and infarct regions, respectively (Table 1). As expected in healthy

control hearts, the four clusters with the highest enrichment scores (ES) were identified with the mitochondria, nucleus, RNA processing, and the innate immune response. In the remote region of the infarcted LV, however, the highest ES scores were displayed by proteins associated with an altered enzymatic activity such as lyases, isomerases, and GTPases, indicative of increased remodeling activity (Dixon and Spinale 2010). Interestingly, the annotation clusters identified in Figure 5. EphrinA1 in the heart. (a) The primary sequence of ephrinA1 with trypsin cleavage sites denoted by underlined lysine (K) or arginine (R) amino acids. Murine sequence NCBI accession NP_034237, generated using the MS-Bridge program at http:// prospector.ucsf.edu/ allowing for one missed cleavage. (b) Expression profile of trypsinized ephrinA1 fragments: matches between theoretical and detected fragments from a control, healthy heart (top), and after acute MI (bottom) are shown. Selected ephrinA1 trypsin fragments that are present in a healthy control heart (m/z = 908, 1632.96, 2816.25, and 4497.11 Da) but not in the region at risk from the infarcted heart are shown border region of the infarcted LV showed high ES for ribosomal proteins, DNA binding, and mRNA processing. These data suggest high transcription and translational activity, which is expected during the healing and regeneration process post-MI (i.e., increased protein turnover) (Guo et al. 2017, Datta et al. 2017). The fourth annotation cluster with the highest ES in the border zone was associated with the defense response, in accordance with inflammation being a fundamental process during the early stages of post-infarction myocardial remodeling (Ma, Yabluchanskiy, and Lindsey 2013, Chen and Frangogiannis 2017). These are activated after ischemia and play an essential role in several pathways to facilitate clearance of apoptotic cells and necrotic tissue, as well as to increase metabolic activity to compensate for the oxygen deprivation and reduced substrate availability. Finally, annotation clusters from the infarcted LV proteins included mitochondrial and metabolic enzymes, lipoproteins, phagocytic vesicles, and

proteins involved in redox processes.

Table 1: Tentative protein identifications in the healthy heart (control) and post-MI regions of interest (remote, border and infarct). Sections underwent trypsin digest for 4 hours.

Regions of interest	Enrichment Score	Pathway	Proteins
Control	1.46	mitochondria	ATP5E, COX7A2, ATP5F1, COX7A2L, CDK5, COX7A2L, HIGD2A, GPX4,
Total clusters 18			CISD2, MRPS28, MCL1, GDAP1, COX7A2, MCL1, GDAP1, ALKBH3, FAM32A
	1.28	nucleosome and methylation	UTP3, HIST1H2AF, HIST2H2AC, HIST1H2AH, H1FOO, CRH, PFN1, MCL1,
			NSD1, SRSF1, GPSM1, PNN
	1.17	RNA processing	SRSF1, YTHDC1, RBMY, RBM28, PNN, PPIG, LARP7, RSL1D1, JAKMIP1
	1.01	innate immune response	DEFB29, DEFB18, DEFB22, RDN, COL4A1, PTN, WNT11, MANF
Remote	2.34	lyases activity	PCBD2, MLYCD, NEIL3, AMD1, AMD2, AUH
Total clusters 30			
	2.14	isomerases	PPIE, PPID, TTC9, PIN4, PBLD2, TRUB1
	1.74	ribosome and mitochondria	QRDL, MRPL52, MRPL21, MLYCD, MTG1, MRPS12, MRPL19, MRM2, SCO2, AUH, GLRX2
			RPS27, RPS27L, SQRDL, PCBD2, RAF1, COMT, CBR2, KRAS, COA5, RAB35, PPID, COA7, RHOA,
			MRPL52, RPS27, MRPL21, MRPS12, MRPL19, RPS27L

	1.41	**GTP-binding**	**RSG1, GIMAP4, RABL3, KRAS, MTG1, RAB35, RASL10B, RHOA, GCH1, OLA1,**
			CNP, SMC2, CHST4, CNP, CDK9, UBE2QL1, **CDKL3, PRKAR2B, REP15, WNT6, TRAPPC3L, PPIE**
Infarct	**8.56**	**mitochondria**	**HCCS, AURKAIP1, MIGA1, GOT2, NDUFS6, CISD2, DNAJC15, DYNLL1, MRPL36, PDHA1,** **HADH,**
Total clusters 61			**MRPL53, NMNAT3, FECH, CYP11A1, ACADS, PLD6, HRK, PFDN2, SLC25A33, UQCRH,** **G0S2,**
			MRPL45, FASTKD5, GATB, TUFM, TXN2, **MTX1, ECHS1, PTPMT1, MRPL20, MRPL15, MRPL18,**
			SLC25A42, AGK, ETFB, ECI1, NDUFA2, SIRT4, MPC1, RAF1, AK4, TRNT1, PRELID1, **RAB32, UCP2,**
			L2HGDH, COA7, ENDOG
	4.83	**dehydrogenases and monooxygenases**	**TUFM, NIT2, VAPB, MME, ECHS1, HSPA1B, PRDX1, PKM, GOT2, GPX1, CISD2, TMED4, DYNLL1,**
			RPL8, RHOA, RPL3, TMED10, PDHA1, HADH, **GAPDH, ETFB, GSTA1, ECI1, RAB8A, NDUFA2,**
			ACADS, AK4, SLC9A3R1, LIN7A, UQCRH, TXNDC5, HAO2, RAB22A, CSTB
			UGDH, RRAD, BLOC1S6, ENO2, GSTA2, KHK, KRT18, HAO2, RPS12
	3.31	**GTP signaling, phagocytic vesicles, and lipoproteins**	**RAB8A, RAB8B, RAB33A, RAB32, DIRAS2, RAB18, PTP4A3, RAB37, RAB22A, RHOA, GNG2,**
			RAB10, GNG4, YKT6, FBXL2 **HCCS, GABARAPL2, HPCAL4, MME,**

			CDC42SE1, ARF6, KCNIP3, GOLGA7, FAM49B, CHIC2, LIME1,
			WNT8A, CIB1, GFRA3, TUFM, GIMAP4, RRAD, AK4, SRPRB, GCH1, RABIF
			HSPA1B, MRPL20, RPL8, MRPL36, ENO2, RPL3, MRPL18, GEMIN2, TGFBR1, VTI1B, H2-AB1,
			ANXA5, TRNT1, RASSF5, MAP3K15, CSTB, VAMP3, FABP2, ELP4, PSTK, GUK1
	3.05	**redox processes**	**STEAP3, STEAP4, LDHB, NDUFA2, LDHA, SDR39U1, CYP11A1, ACADS, TXN2, UGDH, PRDX1, ADI1,**
			NDUFS6, GPX1, L2HGDH, UQCRH, FMO2, HAO2, TXNRD1, GPX8, PDHA1, ALKBH3, HADH, DR9C7,
			ETFB, GAPDH
Border	**10.04**	**Ribosomal proteins**	**RPL18, MRPL52, RPL36A, MRPS33, RPL26, RPS27L, RPL37, RPL24, RPL38, RPL39, MRPL30, RPS8,**
Total clusters 21			**RPL29, RPS26, RPL41, RPL32, RPL32-PS, RPL21, RPS14, FAU, RPS13, RPL7A, MRPL33, RSL24D1**
			SNRPD1, ZCCHC17, SNRPE, EIF3D, HMGB1, MANF, H2AFZ, H3F3A, KRAS, AIF1L, PRPF4B, UBE2L3,
			HIST1H1T, SPCS1, NKIRAS1
	6.12	**DNA binding and nucleosome**	**RPL18, NKAP, PRPF4B, AURKAIP1, RBM7, RPS19BP1, CBX5, EBNA1BP2, HIST1H2BM, H2AFV,**
			MAK16, ELOF1, RBM8A, DNAJC8, H2AFZ, HIST3H2BA, MRPL33, CABLES1, SPATA24, ARGLU1,
			MRPL52, POLR1D, ZCCHC17, HIST1H1T,

			RPS14, LLPH, UBD, RPS13, ING5, THAP7, ING2,
			POLR2K,
			FCF1, RPS26, HIST1H4A, RSL24D1, TCEA2, RPL7A, FAM32A, ARL6IP4, HIST1H2BB, HIST1H2BH,
			MRPL30, UQCC2, SRSF5, RPL21, RSRC1, NOP16, HIST1H3A, HIST1H3B, H3F3A, MPHOSPH6,
			SNRPD1, SOX16, SOX19, HIST1H1B, MXD4, SNRPE, PRPF38A, HMGB1, HMGB3, TCEA3, TNP1,
			UBE2L3, SNURF, SYF2, PRM1, H3F3C, PRM2, SNRNP27, S100A5, RPS27L, MANF, SERF2, RPS8,
	3.66	**mRNA processing**	**HIST1H2BB, HIST1H1B, HIST1H2BH, TNP1, HIST1H2BM, HIST1H1T, H2AFV, HIST1H4A, HIST1H3A,**
			H2AFZ, HIST1H3B, H3F3A, PRM1, H3F3C, PRM2, HIST3H2BA, HMGB1, THAP7, HMGB3, CBX5,
			LLPH, POLR1D, PRPF4B, SNRPD1, ING5, KRAS, MXD4, TCEA3, SOX16, TCEA2, SOX19, SPATA24,
			ING2, RPL26, UBE2L3, TMA7,CXCL14, RBM8A, TCEA2, MPHOSPH6, UBD, RPL29, ING2, POLR2K,
	3.06		**SRSF5, PRPF4B, RBM8A, RSRC1, SNRPD1, SYF2, ARL6IP4, SNRNP27, SNRPE, PRPF38A, POLR2K,**
			DNAJC8, RBMX2, AURKAIP1, CCDC12, RBMX2, THAP7

CHAPTER 4: RELATIVE QUANTITATION OF ENDOGENOUS EPHRINA1 IN CARDIAC TISSUE

INTRODUCTION

EphrinA1, a highly expressed tyrosine kinase receptor-ligand in healthy cardiomyocytes, is reduced following myocardial infarction (MI) (Dries et al., 2011). A single intramyocardial injection of chimeric ephrinA1-Fc at the time of ischemia mitigates the injury in both reperfused and non-reperfused myocardium by reducing apoptosis, necrosis, and inflammation. Previous work from our group has successfully imaged and qualitatively identified endogenous ephrinA1 pre- and post-MI using matrix-assisted laser desorption ionization mass spectrometry imaging (MALDI-MSI) coupled with a time-of-flight mass spectrometer (MALDI/TOF MS). Building on our previous work, we are now focused on understanding and characterizing ephrinA1's role in cardiac tissue by developing an integrated quantitative method to determine endogenous levels of ephrinA1 in cardiac tissue using MALDI-MSI technologies. Herein, we have optimized the methods for the relative quantitation of endogenous tryptic ephrinA1 peptides detected in the healthy murine myocardium. In healthy myocardium, there was approximately 50 ng of endogenous ephrinA1 per tissue section of 9.43 mm^2 average area. MALDI-MSI thus provides a tool for the determination of not only anatomical distribution, but also relative quantitation of endogenous ephrinaA1 in cardiac tissue, advancing our understanding of ephrinA1 expression profile in cardiac tissue.

RESULTS & DISCUSSION

MALDI-MSI optimization for the identification of EphrinA1 in tissues–

Enzymatic digestion has long been used in bottom-up proteomics with trypsin being the gold standard protease (Zhang et al., 2013). Four different experimental conditions of the ephrinA1-His tag standard determined the optimal digestion conditions: 1) concentrations of the standard, 2) concentrations of trypsin, 3) duration of digestion, as well as, 4) in-solution *versus* on-surface digestion. Optimization of trypsin digestion and MALDI matrix conditions were performed to ensure accurate and reproducible identification of ephrinA1-His tag standard's (n=5) tryptic peptides to identify endogenous ephrinA1 in cardiac tissue confidently (n=3).

Table 2 lists a summary of the percent coverage results for ephrinA1-His tag standards that were pipetted directly onto an ITO slide after 4-hour digestion of varying ephrinA1 and trypsin concentrations. The peptides mixed with CHCA only provided a maximum of 9 percent coverage and has a polymerization effect (Fig 8.) . Using the SA matrix with a trypsin concentration of 40 µg/mL, and 100 µg/mL ephrinA1 provided the greatest percent coverage ranging from 19 – 49 percent after 4-hour digestion.

Table 2. Summary of percent coverage for ephrinA1-His tag standards comparing CHCA and SA matrices in two optimization protocols: 100 µg/mL ephrinA1-His tag with varying trypsin concentration (top), and varying ephrinA1-His tag concentration using 40 µg/mL trypsin (bottom).

Matrix	EphrinA1 Concentration	Typsin Concentration	Coverage percentage	Sequence Identified (See Supplemental Table 1)
CHCA	100 µg/mL	20 µg/mL	0-2%	5, 8
CHCA	100 µg/mL	40 µg/mL	0-6%	4, 8,18
CHCA	100 µg/mL	100 µg/mL	0-3%	4, 8, 27
SA	100 µg/mL	20 µg/mL	1-47%	14, 43, 45, 48, 51
SA	100 µg/mL	40 µg/mL	25-65%	4, 7, 11, 13, 16, 18, 22, 26, 29, 32, 39, 43, 44, 45, 46, 47, 48,51, 52, 57, 69, 70, 71, 72
SA	100 µg/mL	100 µg/mL	0-9%	7, 18

Matrix	EphrinA1 Concentration	Typsin Concentration	Coverage percentage	Sequence Identified (See Supplemental Table 1)
CHCA	10 µg/mL	40 µg/mL	1-6%	3, 5, 10
CHCA	25 µg/mL	40 µg/mL	1-12%	4, 5, 6, 10, 19
CHCA	50 µg/mL	40 µg/mL	0-4%	4, 10
CHCA	100 µg/mL	40 µg/mL	0-6%	4, 8, 18
SA	10 µg/mL	40 µg/mL	33-57%	7, 8, 12, 15, 27, 42, 45, 53, 71, 75
SA	25 µg/mL	40 µg/mL	0.05	17
SA	50 µg/mL	40 µg/mL	9-25%	7, 18, 61,
SA	100 µg/mL	40 µg/mL	25-65%	4, 7, 11, 13, 16, 18, 22, 26, 29, 32, 39, 43, 44, 45, 46, 47, 48,51, 52, 57, 69, 70, 71, 72

Experiment utilized three different incubation time points with 40 µg/mL trypsin digestion and 100 µg/mL ephrinA1-His tag: 2, 4, and 8-hrs. As shown in Fig 9 (A-C), the 4-hr digestion provided higher intensity peptide profiles compared to the 2- and 8-hr digestions. The percent coverage for the 2-hr digestion was 15 percent and matched 3 ephrinA1-His tag standard peptides (sequences 2, 6 and 26 in Table 4), whereas the 4-hr digestion provided 65 percent coverage, with

11 peptides matching ephrinA1-His tag standard (sequences 2, 6, 9, 11, 20, 24, 37, 44, 65, 66, and 67 in Table 4), and the 8-hr digest 24 percent coverage with 3 peptides matching ephrinA1-His tag standard (sequences 6, 16 and 38 in Table 4).

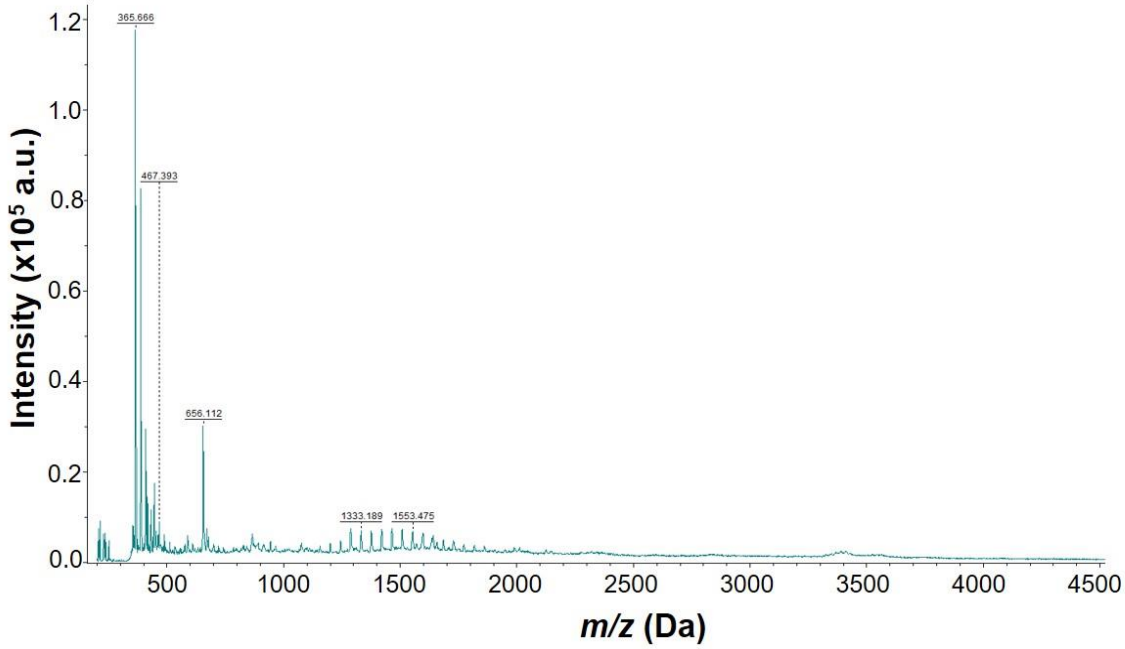

Fig. 8 EphrinA1 mass spectra showing polymerization effect when using CHCA as a matrix.

The 4-hr digestion using SA matrix and 40 µg/mL of trypsin solution, yielded a maximum number of missed cleavages of three. During the process of matrix optimization, we observed the formation of a polymerization interference in the CHCA samples (Fig. 8). Importantly, the effect was not seen when using SA as the matrix (Fig. 9), further supporting SA as the most efficient matrix for studying both ephrinA1-His tag standard and endogenous ephrinA1, at a trypsin concentration of 40 µg/mL.

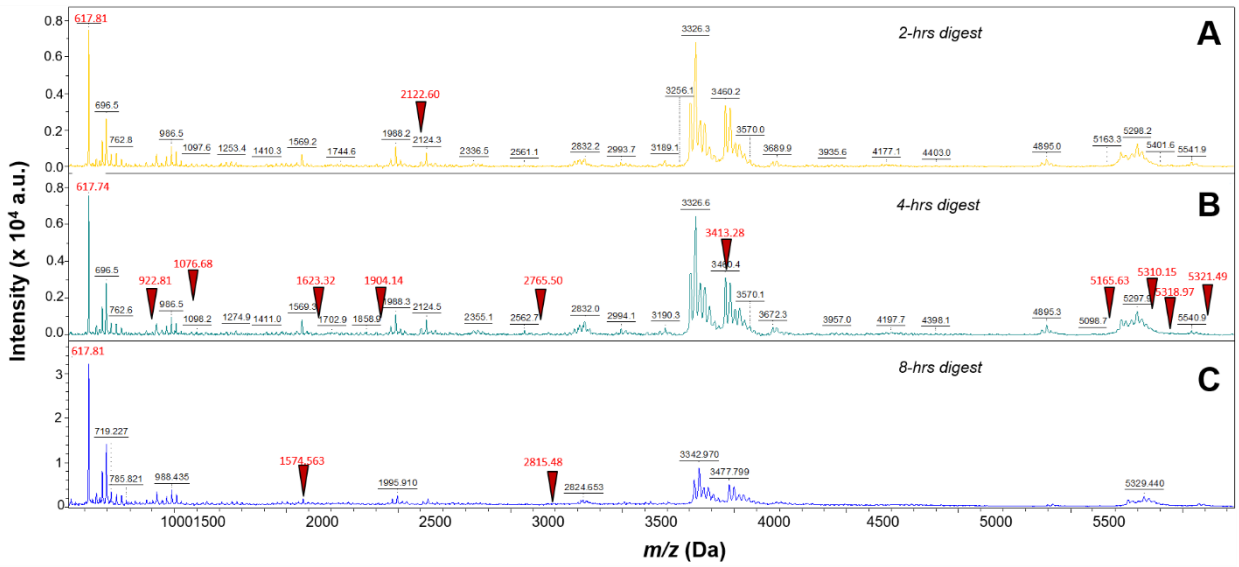

Figure 9. Comparison of ephrinA1-His tag (concentration of 100 µg/mL) *m/z* spectra after a 2- (A), 4- (B), and 8-hrs (C) trypsin digestion (40 µg/mL).

Comparision between the ephrinA1-His tag peptides for native (pipetted on a slide) versus in-solution (denaturing conditions) are shown in Fig. 10 the Venn diagram. Peptides listed under on an ITO slide include both cardiac tissue and ephrinA1-His tag standards; whereas, in-solution digestion only includes ephrinA1-His tag standards. Results found there was only one unique peptide sequence detected from the in-solution digestion; whereas, there was fifteen that overlapped. Moreover, in the cardiac tissue samples and the endogenous standards on the ITO slide, there were eight unique peptides detected. To further understand differences in digestion peptide profiles, we proceeded to dimensionally locate each of the peptide fragments within the cartoon structure of a reported crystal structure for ephrinA1.

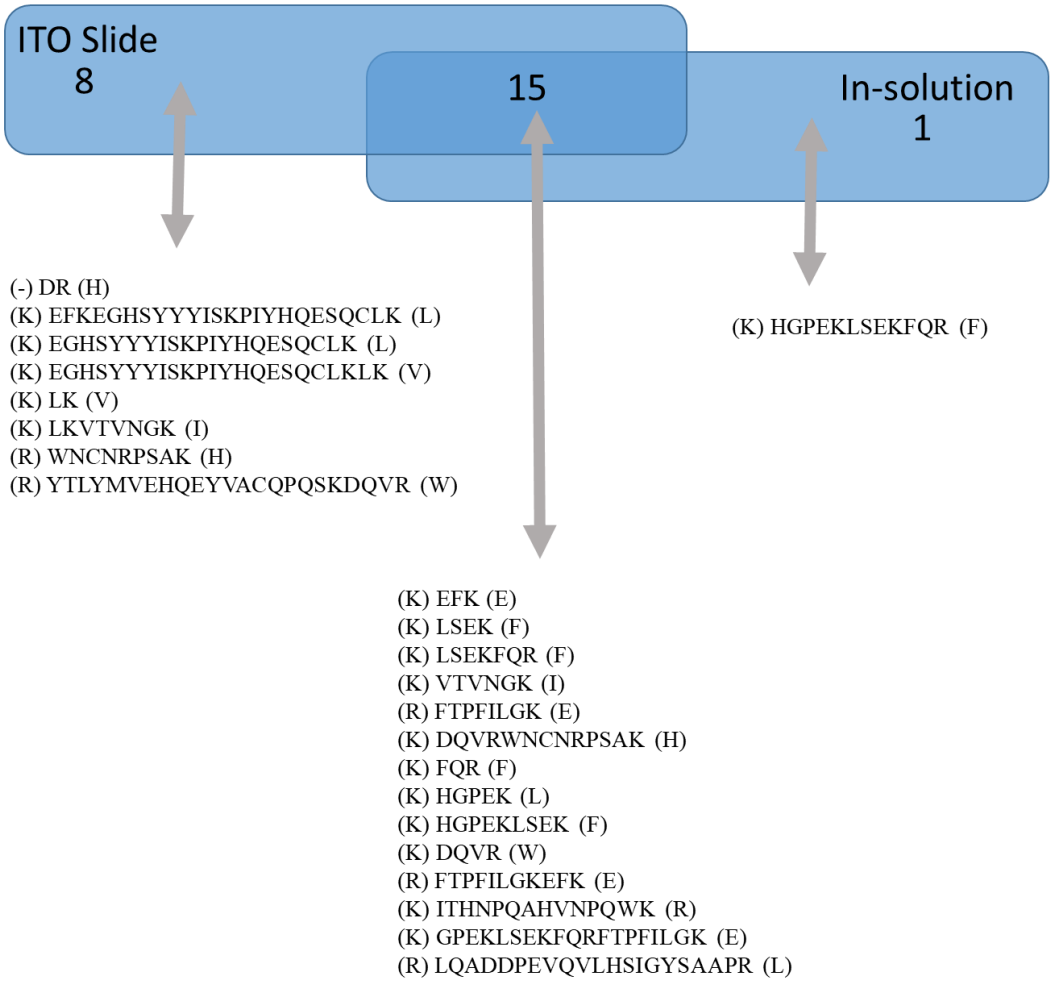

Fig. 10 Venn diagram showing sequences identified in standards samples on ITO slides *versus* peptides detected with in-solution digestion.

EphrinA1 peptides identified in trypsin digests of cardiac tissue–

Fig. 11 identifies peptide sequences found in both cardiac tissue and ephrinA1-His tag standards.

This cartoon model of ephrinA1 depicts the specific sequences of the ephrinA1 tryptic peptides detected in tissue samples and ephrinA1-His tag standards. Peptides identified were primarily

located on the G-H loop where the inherently flexible G-H loop is freely accessible to the trypsin protease. The 17 peptides identified in tissue and the ephrinA1-His tag protein are in Table 4.

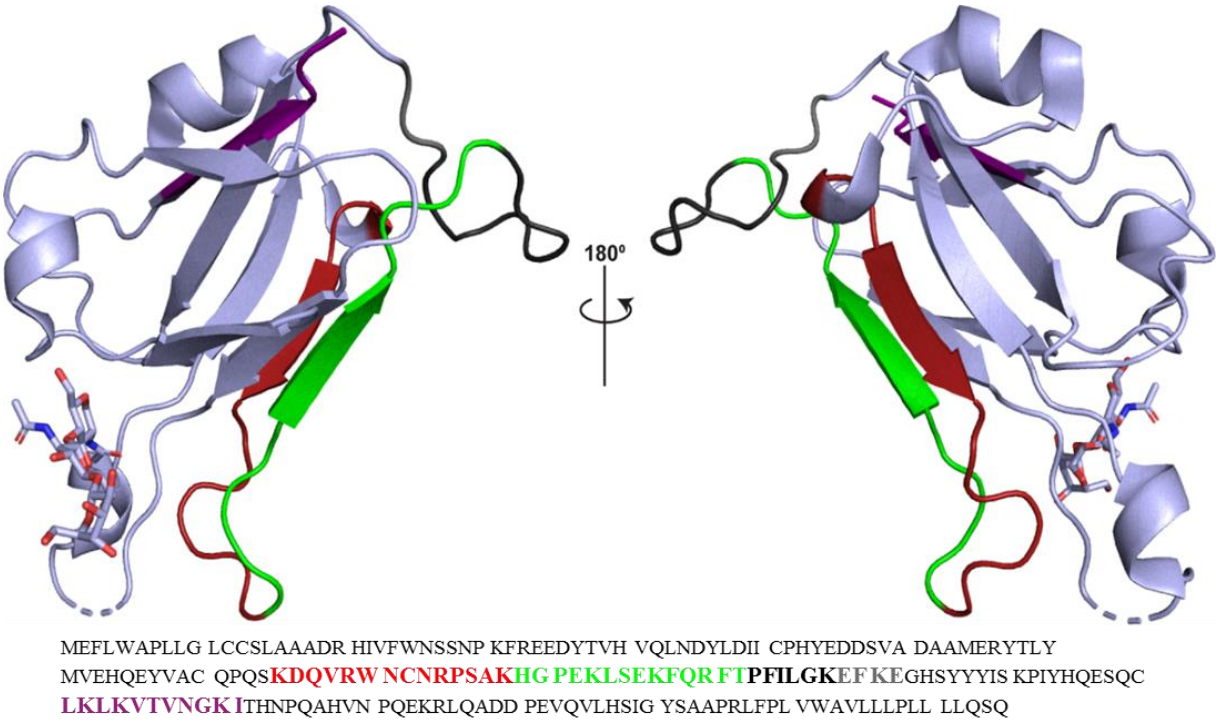

Fig. 11 Cartoon representation of ephrinA1 with peptide fragments identified during imaging experiments in both cardiac tissue and ephrinA1-His tag standards highlighted in the structure with corresponding colors in the sequence. EphrinA1 figure was generated using PyMOL (Pymol reference) and PDB 3CZU (Himanen et al., 2010).

Table 3. Tryptic peptides detected both in cardiac tissue samples and ephrinA1-His tag standard.

Start	End	Observed	Mr(expt)	Mr(calc)	Delta	M	Peptide detected
119	121	423.492	422.4846	422.4755	0.009	0	(K) DQVR (W)
108	110	450.521	449.5136	449.5041	0.01	0	(K) DQVRWNCNRPSAK (H)
104	107	476.553	475.5456	475.5365	0.009	0	(K) EFK (E)
86	89	517.566	516.5586	516.5487	0.01	0	(K) FQR (F)
99	103	567.626	566.6186	566.6074	0.011	0	(K) HGPEK (L)
145	150	617.727	616.7196	616.7076	0.012	0	(K) HGPEKLSEK (F)

143	150	859.063	858.0556	858.0375	0.018	1	(K) HGPEKLSEKFQR (F)
104	110	908.051	907.0436	907.0253	0.018	1	(K) HGPEKLSEKFQRFTPFILGK (E)
111	118	923.15	922.1426	922.121	0.022	0	(K) ITHNPQAHVNPQWK (R)
99	107	1025.153	1024.146	1024.129	0.017	1	(K) LSEK (F)
90	98	1076.229	1075.222	1075.202	0.02	0	(K) LKVTVNGK (I)
111	121	1327.619	1326.612	1326.581	0.03	1	(K) LSEKFQR (F)
99	110	1456.654	1455.647	1455.617	0.029	2	(K) VTVNGK (I)
86	98	1574.772	1573.765	1573.735	0.03	1	(R) FTPFILGK (E)
151	164	1613.784	1612.777	1612.745	0.032	0	(R) FTPFILGKEFK (E)
166	186	2267.519	2266.512	2266.466	0.046	0	(R) LQADDPEVQVLHSIGYSAAPR (L)
99	118	2360.782	2359.775	2359.723	0.052	3	(R) WNCNRPSAK (H)

Relative quantitation of EphrinA1 using MALDI-MSI–

Comparison of cardiac tissue expression profiles - determined for the imaged area (Fig 12) - to the intensity profile distribution of ephrinA1-His tag standards allowed for the relative quantification of endogenous ephrin A1 expression. Increasing ephrinA1 concentrations corresponded to a non-linear increase of the mean intensity profiles; the nonlinear response, however, is most likely attributable to matrix selection (Parker et al., 2008), (Knochenmuss et al., 1998), and (Schlosser et al., 2005). Ion suppression due to matrices presents a significant challenge with MALDI/MSI of complex biological samples due to the chemical interferences from the matrix and the diverse components in the sample itself (Szájli et al., 2008, Prentice et al., 2017). While necessary for relative quantification purposes, the complete digestion of native proteins in tissue samples by trypsin is difficult compared to digestions of denatured proteins; performing native protein digestion often results in numerous missed cleavage sites. Missed cleavages arise from secondary

and tertiary structural elements of the protein limiting trypsin's accessibility to Arg and Lys residues. As we expected (Fig 11, Table 3), MALDI-MSI consistently detected only 17 of the 75 possible ephrin A1 peptide fragments determined from theoretical, full digestion of the protein. These 17 consistently identified peptides became the signature fragments and focus for relative quantitation.

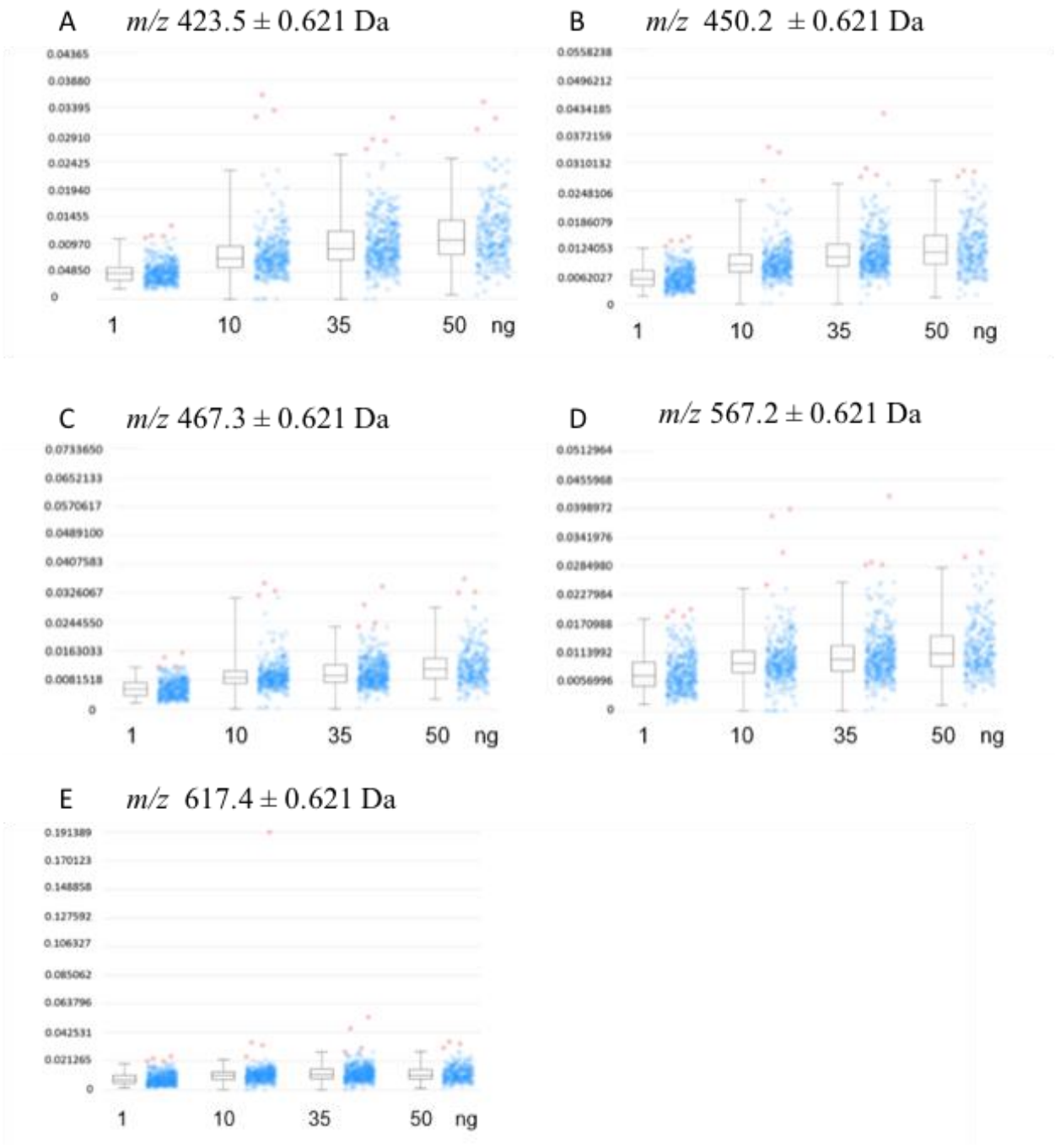

Fig. 12 Intensity distribution for the tryptic fragments *m/z* 423.5, 450.3, 476.3, 567.2 and 617.4 Da show expression profiles of standards at 1 ng, 10 ng, 35 ng, and 50 ng (A-E), respectively.

Relative quantitation of all ephrinA1 peptides is summarized in Fig. 12-14. Reconstructed

chemical ion images (Fig. 13) of tryptic peptides shown in both endogenous ephrinA1 as well as the ephrinA1-His tag standard indicate that endogenous levels of ephrinA1 are approximately 50 ng per section in healthy murine cardiac tissue.

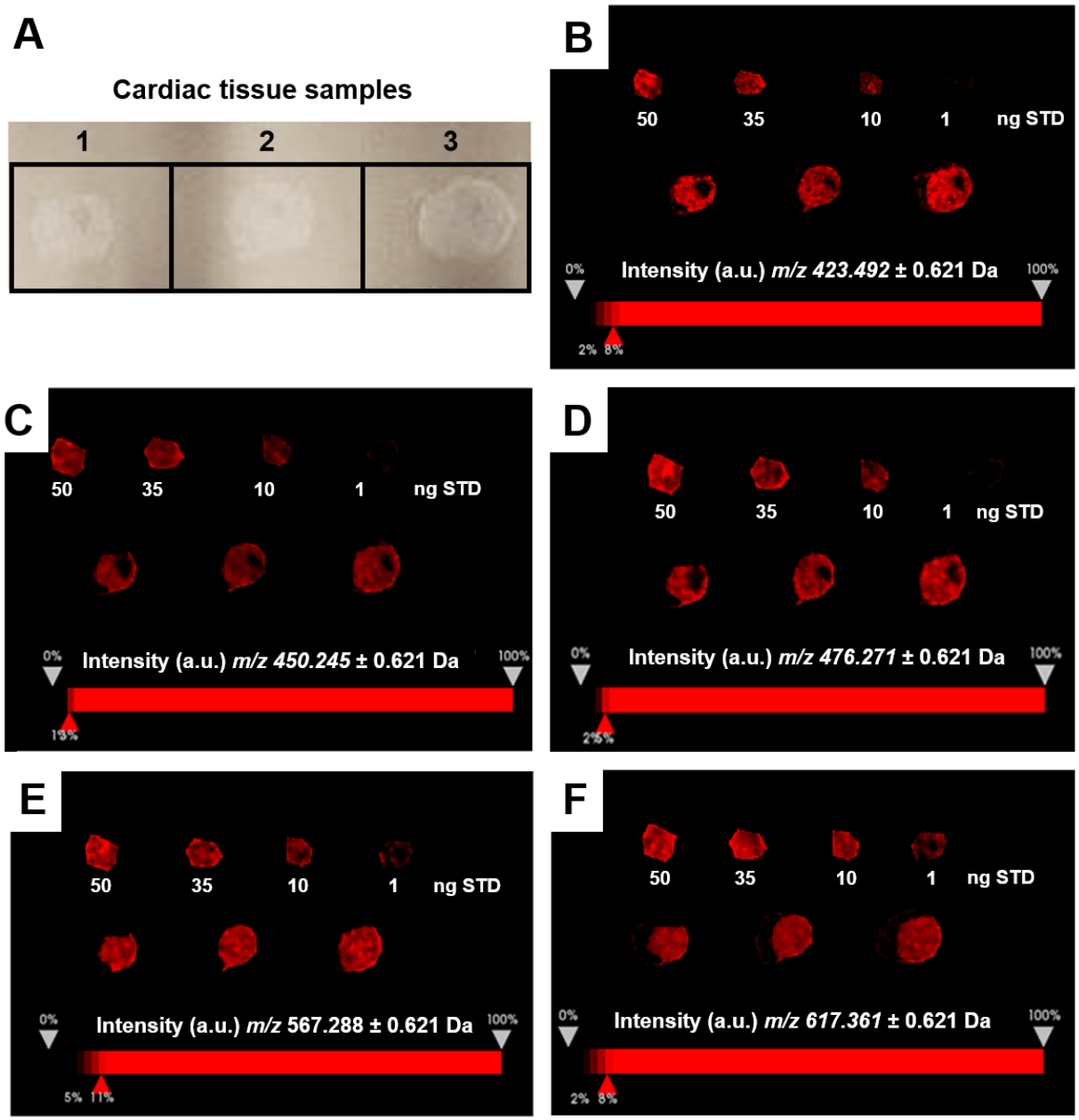

Fig. 13. Ion Images of EphrinA1 Peptides for Relative Quantitation. (A) Image of samples on ITO slide. (B-F) Reconstructed chemical ion images of the EphrinA1-tryptic peptides, *m/z* 423.5 (B), 450.2 (C), 476.3 (D), 567.2 (E), and 617.4 (F)

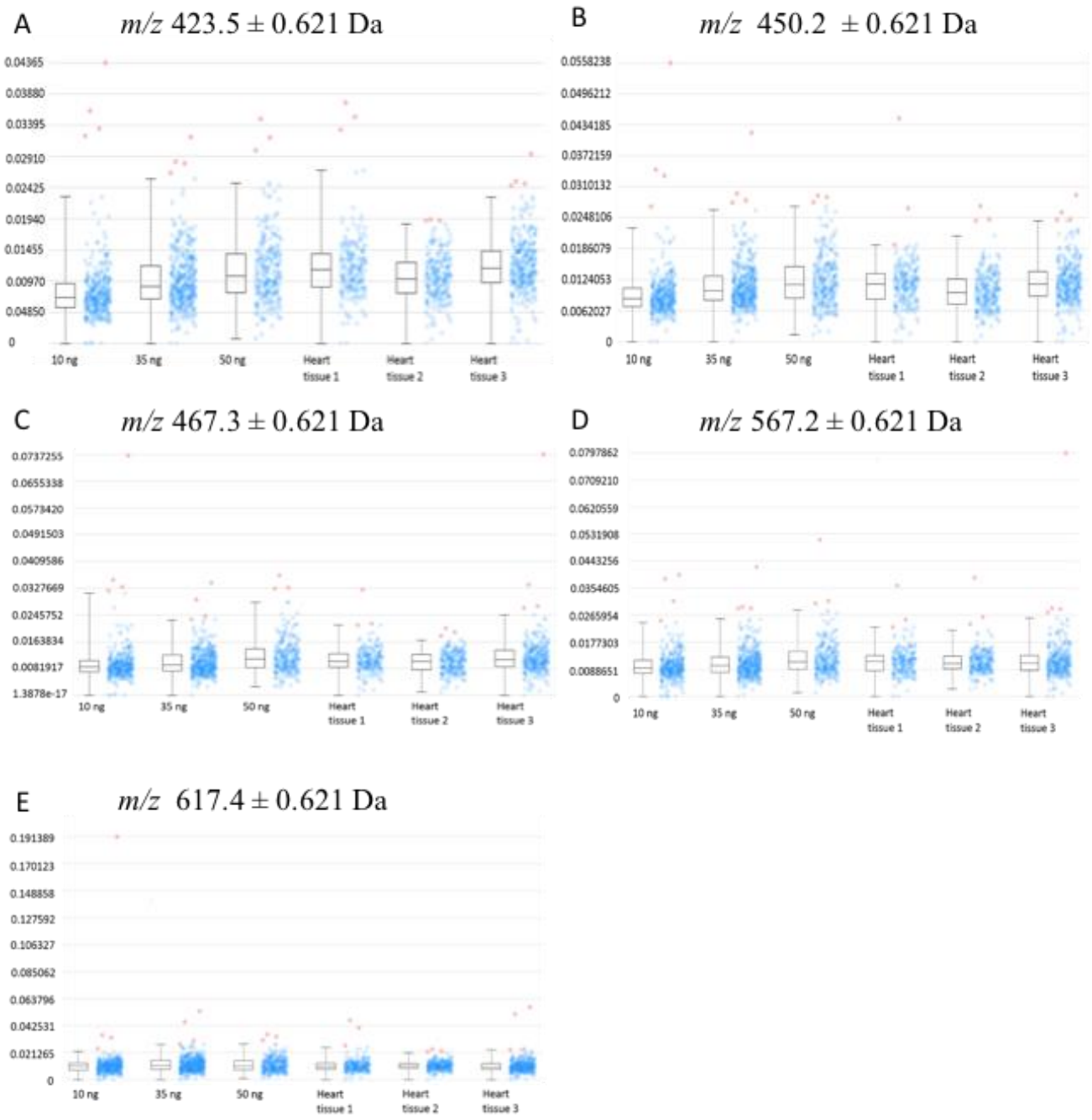

Fig. 14 Concentration distribution for ephrinA1-His tag standard tryptic peptide fragments for *m/z* 423.5, 450.3, 476.3, 567.2 and 617.4 Da show expression profiles comparing analytical his tag standards at 10 ng, 35 ng, and 5 ng against expression profiles of 3 independent samples of healthy cardiac tissue.

Table 4. Sequences of ephrinA1 tryptic peptides identified from analytical standards and cardiac tissue and which matrix that was used to identify each.

Sequence Number	Sequence	Matrix
1	(-)DR(H)	
2	(K)LV(V)	
3	(K)EFK(E)	CHCA
4	(K)FQR(F)	CHCA/SA
5	(K)LSEK(F)	CHCA
6	(K)DQVR(W)	CHCA
7	(K)HGPEK(L)	SA
8	(K)VTVNGK(I)	CHCA/SA
9	(K)LKVTVNGK(I)	
10	(K)LSEKFQR(F)	CHCA
11	(R)FTPFILGK(E)	SA
12	(K)HGPEKLSEK(F)	SA
13	(R)WNCNRPSAK(H)	SA
14	(R)FTPFILGKEFK(E)	SA
15	(R)HIVFWNSSNPK(F)	SA
16	(K)FQRFTPFILGK(E)	SA
17	(K)HGPEKLSEKFQR(F)	SA
18	(K)DQVRWNCNRPSAK(H)	CHCA/SA
19	(-)DRHIVFWNSSNPK(F)	CHCA
20	(K)ITHNPQAHVNPQEK(R)	
21	(R)WNCNRPSAKHGPEK(L)	
22	(R)HIVFWNSSNPKFR(E)	SA
23	(K)FQRFTPFILGKEFK(E)	
24	(K)ITHNPQAHVNPQEKR(L)	
25	(K)LSEKFQRFTPFILGK(E)	
26	(-)DRHIVFWNSSNPKFR(E)	SA

27	(R)WNCNRPSAKHGPEKLSEK(F)	CHCA/SA
28	(K)DQVRWNCNRPSAKHGPEK(L)	
29	(K)VTVNGKITHNPQAHVNPQEK(R)	SA
30	(K)LSEKFQRFTPFILGKEFK(E)	
31	(R)YTLYMVEHQEYVACQPQSK(D)	
32	(K)HGPEKLSEKFQRFTPFILGK(E)	SA
33	(K)VTVNGKITHNPQAHVNPQEKR(L)	
34	(K)LKVTVNGKITHNPQAHVNPQEK(R)	
35	(R)WNCNRPSAKHGPEKLSEKFQR(F)	
36	(K)EGHSYYYISKPIYHQESQCLK(L)	
37	(K)DQVRWNCNRPSAKHGPEKLSEK(F)	
38	(K)LKVTVNGKITHNPQAHVNPQEKR(L)	
39	(K)HGPEKLSEKFQRFTPFILGKEFK(E)	SA
40	(K)EGHSYYYISKPIYHQESQCLKLK(V)	
41	(R)YTLYMVEHQEYVACQPQSKDQVR(W)	
42	(K)EFKEGHSYYYISKPIYHQESQCLK(L)	SA
43	(K)DQVRWNCNRPSAKHGPEKLSEKFQR(F)	SA
44	(K)EFKEGHSYYYISKPIYHQESQCLKLK(V)	SA
45	(R)LQADDPEVQVLHSIGYSAHHHHHHHHHH(-)	SA
46	(K)EGHSYYYISKPIYHQESQCLKLKVTVNGK(I)	
47	(R)WNCNRPSAKHGPEKLSEKFQRFTPFILGK(E)	SA
48	(K)RLQADDPEVQVLHSIGYSAHHHHHHHHHH(-)	SA
49	(K)EFKEGHSYYYISKPIYHQESQCLKLKVTVNGK(I)	
50	(R)WNCNRPSAKHGPEKLSEKFQRFTPFILGKEFK(E)	
51	(R)EEDYTVHVQLNDYLDIICPHYEDDSVADAAMER(Y)	SA
52	(R)YTLYMVEHQEYVACQPQSKDQVRWNCNRPSAK(H)	SA
53	(R)FTPFILGKEFKEGHSYYYISKPIYHQESQCLK(L)	SA
54	(K)DQVRWNCNRPSAKHGPEKLSEKFQRFTPFILGK(E)	
55	(R)FTPFILGKEFKEGHSYYYISKPIYHQESQCLKLK(V)	

56	(K)FREEDYTVHVQLNDYLDIICPHYEDDSVADAAMER(Y)	
57	(K)FQRFTPFILGKEFKEGHSYYYISKPIYHQESQCLK(L)	SA
58	(R)YTLYMVEHQEYVACQPQSKDQVRWNCNRPSAKHGPEK(L)	
59	(K)FQRFTPFILGKEFKEGHSYYYISKPIYHQESQCLKLK(V)	
60	(R)FTPFILGKEFKEGHSYYYISKPIYHQESQCLKLKVTVNGK(I)	
61	(K)LSEKFQRFTPFILGKEFKEGHSYYYISKPIYHQESQCLK(L)	SA
62	(R)YTLYMVEHQEYVACQPQSKDQVRWNCNRPSAKHGPEKLSEK(F)	
63	(K)EGHSYYYISKPIYHQESQCLKLKVTVNGKITHNPQAHVNPQEK(R)	
64	(K)LSEKFQRFTPFILGKEFKEGHSYYYISKPIYHQESQCLKLK(V)	
65	(K)ITHNPQAHVNPQEKRLQADDPEVQVLHSIGYSAHHHHHHHHHH(-)	
66	(K)FQRFTPFILGKEFKEGHSYYYISKPIYHQESQCLKLKVTVNGK(I)	
67	(K)EGHSYYYISKPIYHQESQCLKLKVTVNGKITHNPQAHVNPQEKR(L)	
68	(R)YTLYMVEHQEYVACQPQSKDQVRWNCNRPSAKHGPEKLSEKFQR(F)	
69	(K)HGPEKLSEKFQRFTPFILGKEFKEGHSYYYISKPIYHQESQCLK(L)	SA
70	(K)EFKEGHSYYYISKPIYHQESQCLKLKVTVNGKITHNPQAHVNPQEK(R)	SA
71	(R)HIVFWNSSNPKFREEDYTVHVQLNDYLDIICPHYEDDSVADAAMER(Y)	SA
72	(K)EFKEGHSYYYISKPIYHQESQCLKLKVTVNGKITHNPQAHVNPQEKR(L)	SA
73	(K)VTVNGKITHNPQAHVNPQEKRLQADDPEVQVLHSIGYSAHHHHHHHHHH(-)	
74	(-)DRHIVFWNSSNPKFREEDYTVHVQLNDYLDIICPHYEDDSVADAAMER(Y)	
75	(K)LKVTVNGKITHNPQAHVNPQEKRLQADDPEVQVLHSIGYSAHHHHHHHHHH(-)	SA

CHAPTER 5: PRELIMINARY COMPARATIVE EXPRESSION LEVELS OF ENDOGENOUS EPRHINA1 IN CARDIAC TISSUE ACROSS MULTIPLE DAYS POST-MI IN BOTH MALE AND FEMALE MICE

INTRODUCTION

Spatial location and expression profiles determined by MALDI-MSI provided valuable information as to how endogenous ephrinA1 was behaving in cardiac tissue both in healthy control tissue and post-MI. To further investigate ephrinA1 in cardiac tissue the development of a relative quantitation method for endogenous protein in tissue using MALDI-MSI advanced an already invaluable technique. Previous work in chapter 4 has shown the optimization and development of such a method specifically for endogenous ephrinA1 in cardiac tissue. To investigate how ephrinA1-Fc can be used as a novel therapeutic it is necessary to delve deeper and gain insight as to how cardiac tissue is affected post-MI by this treatment. Literature shows there are sex differences between males and females in their response to myocardial infarction as well as in the morality rates (Vaccarino et al 1995, Jneid et al., 2008, Leifheit-Limson et al., 2015). In this study, we aim to shed light on the effects of ephrinA1-Fc as a therapeutic and explore its effect between sexes across time points of 1, 2, 4, and 7 days post-MI.

RESULTS & DISCUSSION

Previous experiments have shown that animals that experience a myocardial infarction and receive treatment of ephrinA1-Fc have improved cardiac function as compared to those that do not receive the treatment. Echocardiographs from these experiments indicate that ephrinA1-Fc treated animals have significantly higher ejection fraction and fractional shortening at both 24-hr and 4 day time points as compared to IgG treated animals, however these studies have thus far only included male mice (P. DuSablon et al. 2017, Dries, Kent, and Virag 2011). In order to determine possible sex differences, both male and female mice were used in this study.

Tables 5 and 6 display combined male and female echocardiography for ephrinA1-Fc treated groups and IgG treated groups. In these experiments, Table 5 (IgG treatment group) shows a possible trend of higher ejection fraction and fractional shortening for females at 1-day post-MI as compared to males. Similar results are seen in the 2-day post-MI group receiving IgG treatment. As the time points extend to 4 and 7 days post-MI it is noticed that the male mice have higher ejection fraction and fractional shortening as compared to the females. As Table 6 indicates, the data is reverse as seen in the IgG treatment groups for the 1 and 2-day ephrinA1-Fc treated groups with ejection fraction and fractional shortening being higher in the male mice than female mice. Interestingly, for the 4 and 7-day post-MI time points the female animals show a higher ejection fraction and fractional shortening as compared to their male counterparts that have received ephrinA1-Fc treatment. Currently, the number of animals in each group is relatively small, to address this more animals will be added to each group in order to determine trends and statistical differences for each group and time point, furthermore, these data were determined using M-mode analysis, B-mode analysis will be conducted in the future.

Table 5. IgG treated mice M-mode echo. Echo analysis collected using M-mode for determining cardiac function of IgG treated animal's post-MI.

IgG treated	Male 1 Day (n=5)	Female 1 Day (n=4)	Male 2 Day (n=4)	Female 2 Day (n=3)
LV Diastolic Volume (µL)	56.69 ± 17.57	50.75 ± 7.89	55.47 ± 10.80	56.14 ± 25.55
LV Systolic Volume (µL)	38.22 ± 13.24	29.40 ± 9.35	36.55 ± 12.60	38.37 ± 25.75
Ejection Fraction (%)	35.52 ± 8.91	45.71 ± 13.82	39.30 ± 10.40	45.12 ± 17.14
Fractional Shortening (%)	17.37 ± 5.10	24.83 ± 10.20	19.31 ± 5.38	23.49 ± 10.31
LVIDs (mm)	38.22 ± 13.24	2.64 ± 0.45	2.92 ± 0.43	2.78 ± 0.86
LVIDd (mm)	3.50 ± 0.48	3.47 ± 0.22	3.57 ± 0.32	3.49 ± 0.66

IgG treated	Male 4 Day (n=2)	Female 4 Day (n=1)	Male 7 Day (n=3)	Female 7 Day (n=1)
LV Diastolic Volume (µL)	31. 98 ± 11.96	60.15	63.16 ± 19.86	91.12
LV Systolic Volume (µL)	19.86 ± 11.91	38.53	30.73 ± 14.19	54.86
Ejection Fraction (%)	45.73 ± 16.43	35.95	59.49 ± 14.26	39.8
Fractional Shortening (%)	22.56 ± 9.25	16.89	33.68 ± 11.40	19.26
LVIDs (mm)	2.27 ± 0.61	3.12	2.59 ± 0.72	3.61
LVIDd (mm)	2.88 ± 0.44	3.75	3.23 ± 0.55	4.47

Sham	Male Sham (n=6)	Female Sham (n=4)
LV Diastolic Volume (µL)	33.85 ± 3.28	17.77 ± 1.33
LV Systolic Volume (µL)	4.23 ± 1.0	1.11 ± 0.49
Ejection Fraction (%)	88.09 ± 2.54	94.12 ± 2.28
Fractional Shortening (%)	58.04 ± 4.48	67.78 ± 4.48
LVIDs (mm)	01.25 ± 0.14	0.74 ± 0.12
LVIDd (mm)	2.94 ± 0.12	2.27 ± 0.07

Table 6. EphrinA1-Fc treated mice M-mode echo. M-mode echo analysis for determining cardiac function of ephrinA1-Fc treated animal's post- MI.

EphrinA1-Fc treated	Male 1 Day (n=1)	Female 1 Day (n=4)	Male 2 Day (n=4)	Female 2 Day (n=2)
LV Diastolic Volume (µL)	56.24	65.78 ± 1.33	57.72 ± 4.87	59.36 ± 6.73
LV Systolic Volume (µL)	16.31	39.44 ± 9.54	31.38 ± 7.66	41.71 ± 4.89
Ejection Fraction (%)	70.99	42.07 ± 6.32	46.36 ± 10.31	29.78 ± 0.21
Fractional Shortening (&)	39.78	20.59 ± 3.51	23.89 ± 6.86	13.65 ± 0.077
LVIDs (mm)	2.2	3.09 ± 0.29	2.83 ± 0.33	2.83 ± 0.33
LVIDd (mm)	3.65	3.87 ± 0.21	3.68 ± 0.13	3.68 ± 0.13

EphrinA1-Fc treated	Male 4 Day (n=4)	Female 4 Day (n=3)	Male 7 Day (n=4)	Female 7 Day (n=4)
LV Diastolic Volume (µL)	103.43 ± 12.41	37.55 ± 13.68	107.18 ± 27.25	82.80 ± 23.74
LV Systolic Volume (µL)	72.34 ± 9.75	19.15 ± 7.84	75.26 ± 26.90	52.17 ± 19.55
Ejection Fraction (%)	30.45 ± 2.77	49.83 ± 2.61	36.63 ± 9.63	43.48 ± 10.22
Fractional Shortening (%)	14.33 ± 1.41	24.36 ± 1.26	18.05 ± 5.09	22.18 ± 6.45
LVIDs (mm)	4.02 ± 0.23	2.30 ± 0.40	3.90 ± 0.68	3.33 ± 0.61
LVIDd (mm)	4.69 ± 0.24	3.03 ± 0.47	4.67 ± 0.56	4.17 ± 0.51

EphrinA1-Fc treated	Male Sham (n=6)	Female Sham
LV Diastolic Volume (µL)	33.85 ± 3.28	17.77 ± 1.33
LV Systolic Volume (µL)	4.23 ± 1.0	1.11 ± 0.49
Ejection Fraction (%)	88.09 ± 2.54	94.12 ± 2.28
Fractional Shortening (%)	58.04 ± 4.48	67.78 ± 4.48
LVIDs (mm)	01.25 ± 0.14	0.74 ± 0.12
LVIDd (mm)	2.94 ± 0.12	2.27 ± 0.07

Intensity box plots (Fig.17-26) as well as ion expression images (Fig. 15-16) were generated using MALDI-MSI and SCiLS lab. Data shown (n=2) indicates that in healthy control murine cardiac tissue that males have on average a higher mean expression of endogenous ephrinA1 than females for the detected peptides (Fig. 17-18).

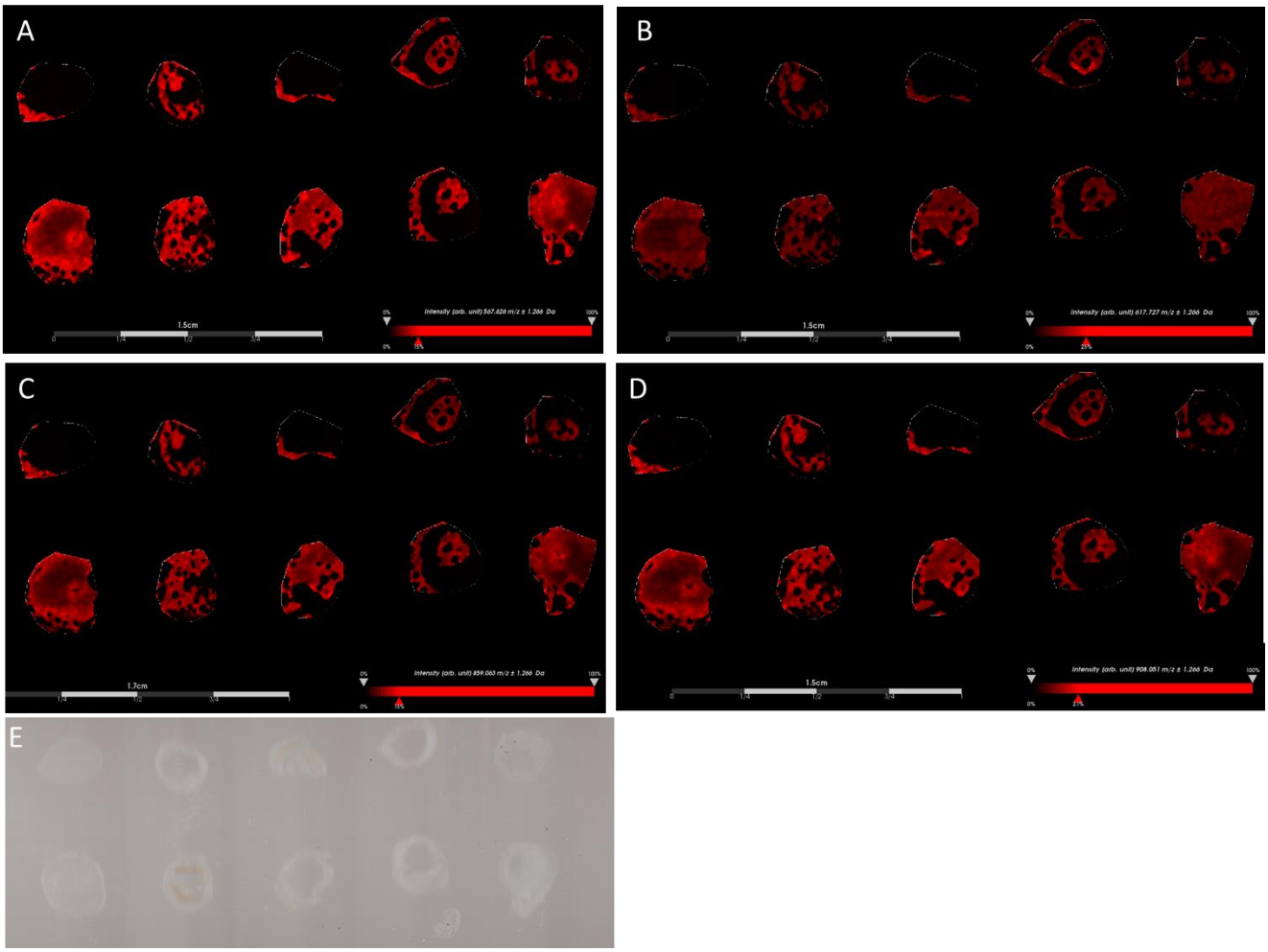

Figure 15. Chemical Ion imges for IgG treated females and males post MSI Endogenous ephrinA1 expression in IgG treated Females (top) and Males (bottom) for control, 1D, 2D, 4D and 7D (left to right respectively) for m/z 567.6 (A), 617.7 (B), 859.1 (C), 908.1 (D) and the scanned tissue sections (E).

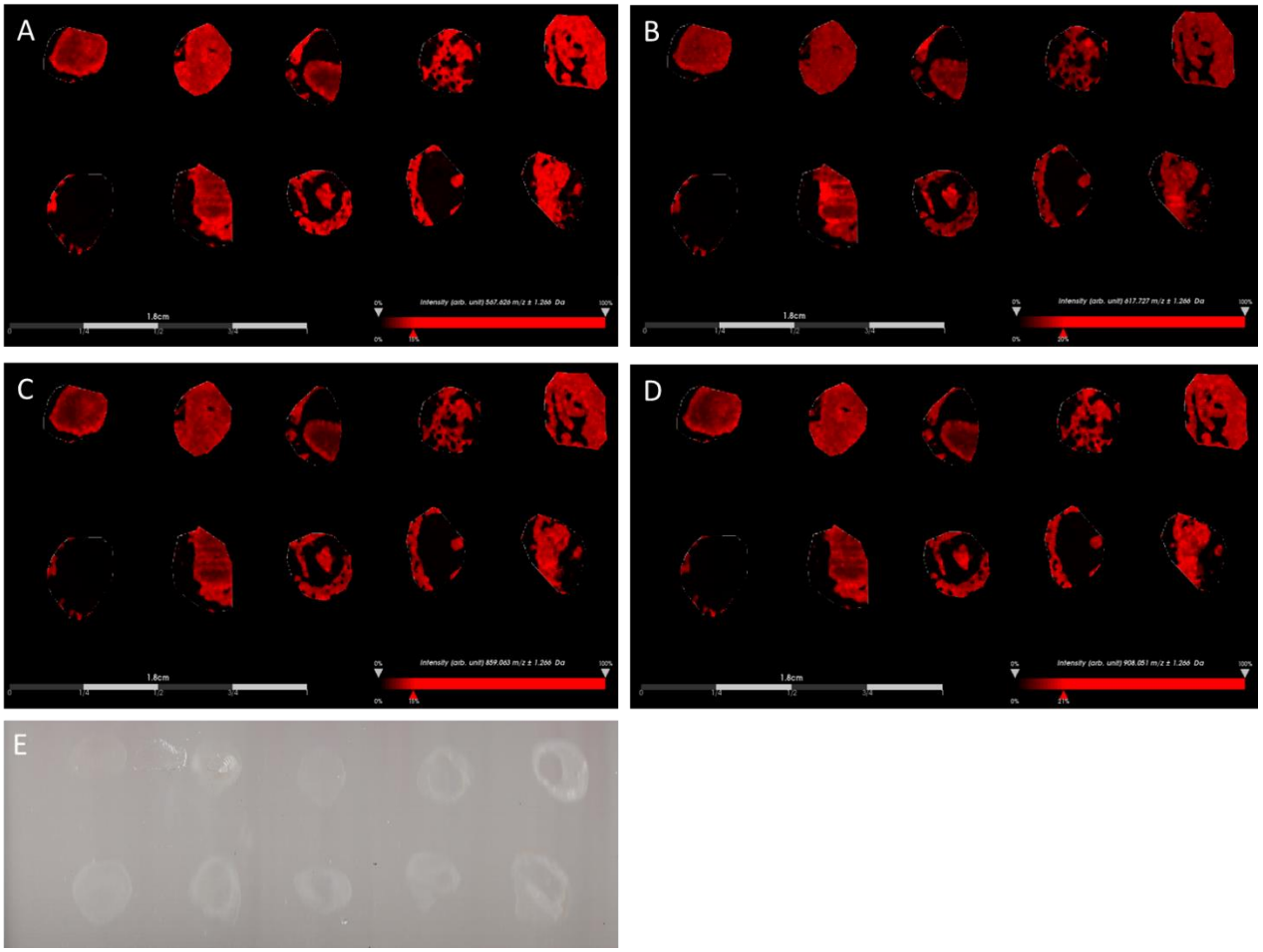

Figure 16. Chemical Ion imges for ephrinA1-Fc treated females and males post MSI. Endogenous ephrinA1 expression in ephrinA1-Fc Females (top) and Males (bottom) for control, 1, 2, 4, and 7 days post-MI (left to right respectively) for m/z 567.6 (A), 617.7 (B), 859.1 (C), 908.1 (D) and the scanned tissue sections (E)..

As Fig 18. depicts IgG treated mice average mean intensities are similar in those ions shown. Although the average mean intensities are similar it is shown that post-MI there are lower average intensities for both males and females at all time points when compared to non-injured control. This data supports and confirms previous data shown in (Lefcoski et al. 2018) that endogenous ephrinA1 levels are decreased at 4 days post-MI. At 1 and 7-day, post-MI with IgG treatment Fig 18. suggests that male mice have a slightly higher endogenous ephrinA1 expression that females, however his is not the case at 2 and

4-day time points where the female group is shown to have slightly higher average mean intensity that the male group for those peptides selected.

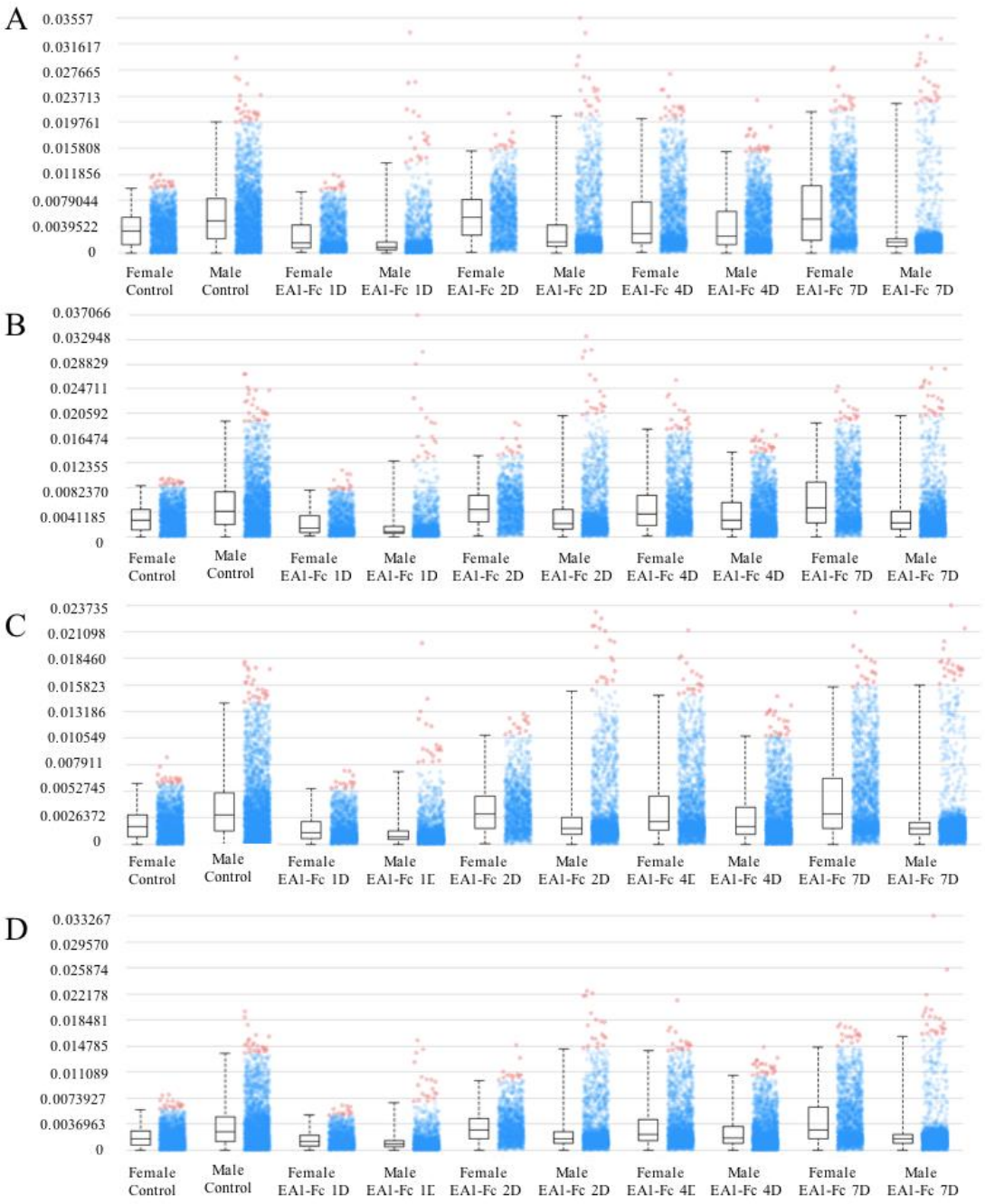

Figure 17. Male and Female EphrinA1 Expression Comparison Box Plots Post-MI EphrinA1-Fc Treated. Box plots comparing ephrinA1-Fc treated males and females at time points 1, 2, 4, and 7 days post-MI for *m/z* 567.6 (A), 617.7 (B), 859.1 (C), and 908.1(D)

EphrinA1-Fc treated animals average mean intensity are shown in Fig 19. Animals that were treated with IgG showed a decrease in average mean intensity for all time points in both sexes of endogenous ephrinA1, this however is not found for in the female ephrinA1-Fc treated animals. At time points 2, 4, and 7 days post-MI average mean intensity is higher in those peptides analyzed than in the non-injured control. Female mice at all time points post-MI show a higher average mean intensity than their male counterparts when receiving ephrinA1-Fc treatment.

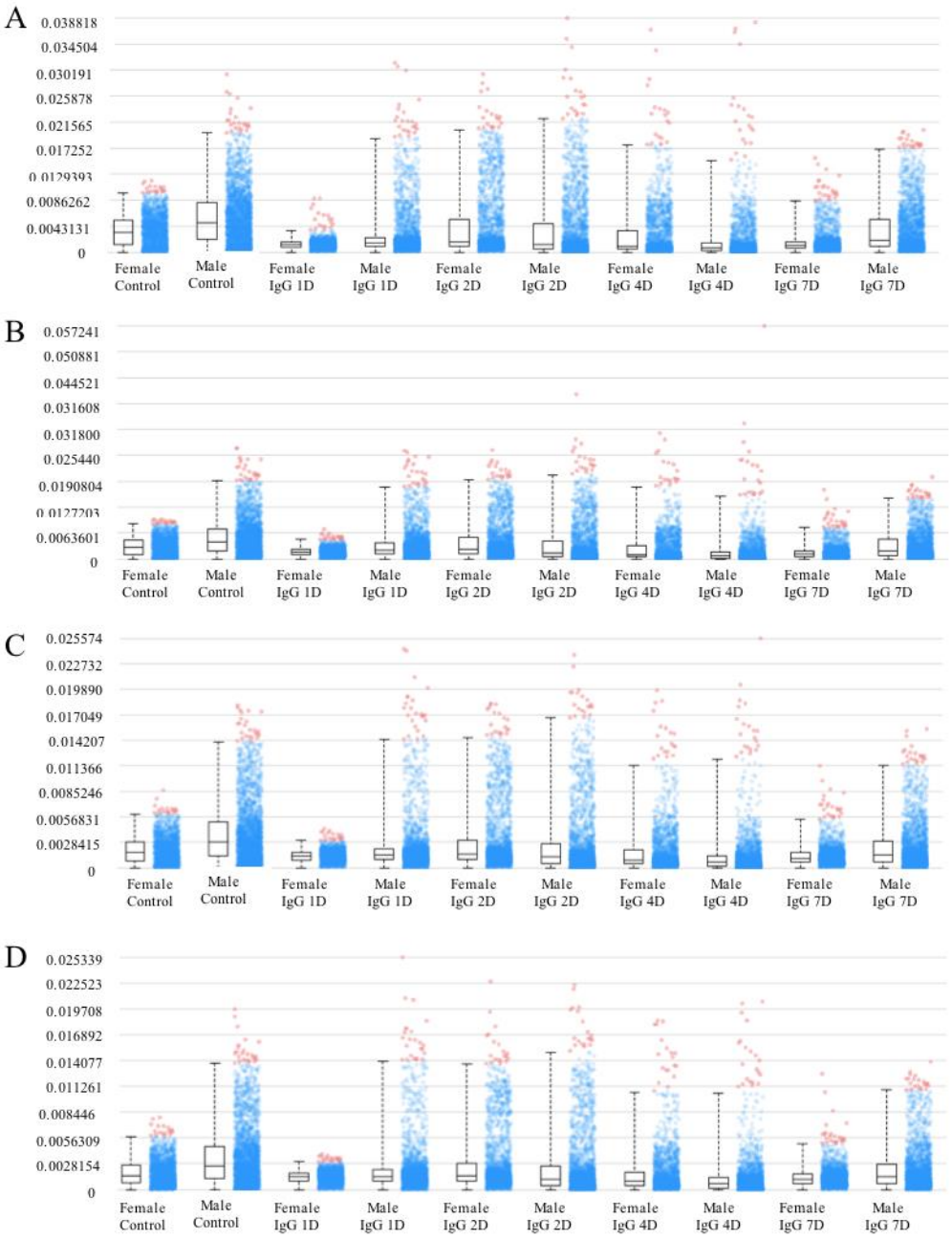

Figure 18. Male and Female EphrinA1 Expression Comparison Box Plots Post-MI IgG Treated. Box plots comparing IgG treated males and females at time points 1, 2, 4, and 7 days post-MI for m/z 567.6 (A), 617.7 (B), 859.1 (C), and 908.1(D)

Comparisons between female non-injured control, ephrinA1-Fc, and IgG treated mice are shown in Figs 19, 21, 23, and 25. As indicated in Fig 29. female average mean intensity for endogenous ephrinA1 peptides at 1-day post-MI are lower in both treatment groups, however the ephrinA1-Fc treatment group more has a lower intensity than that of the IgG groups in three of the four peptides analyzed. For those 2-day, post-MI females (Fig. 21) average mean intensity of endogenous ephrinA1 peptides are higher in the ephrinA1-Fc group than in the healthy non-injured control and the IgG group. The 2-day IgG treatment group retains similar average mean intensity to that of the non-injured control group. In three of the four peptides analyzed at the 4-day post-MI time point (Fig. 23) it is again showed that the ephrinA1-Fc treatment group has an average mean intensity that is higher than both the non-injured and IgG treatment groups. In contrast to the 2-day time point there is larger discrepancy between the non-injured and IgG treatment groups. Similarly, to the 2 and 4-day time points the 7-day time point (Fig. 25) indicates a higher average mean intensity for the ephrinA1-Fc treated group. The same trends are seen with the IgG treatment group showing lower average mean intensity than that of the non- injured control as expected.

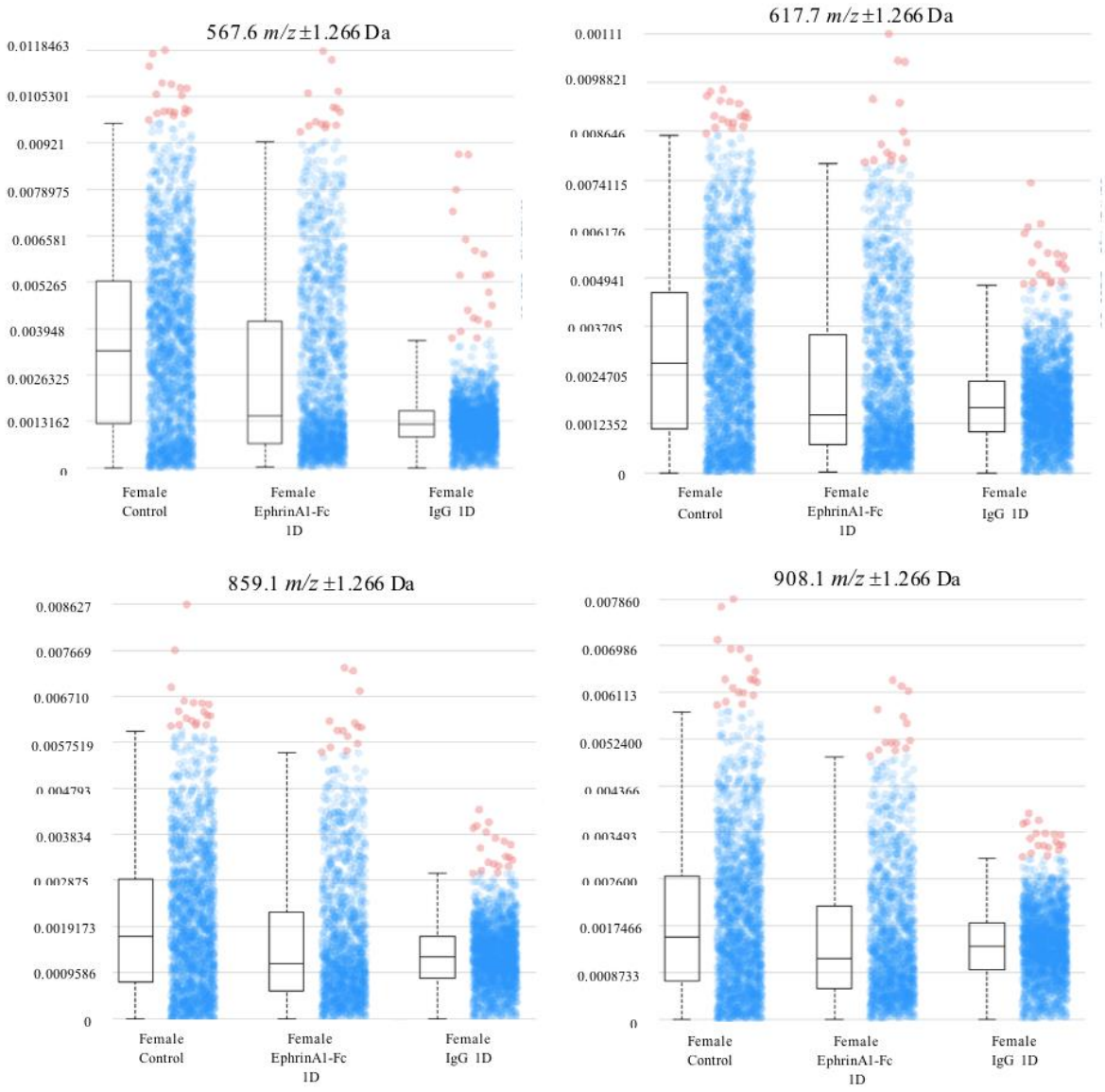

Figure 19. 1 Day Female EphrinA1 Expression Box Plots Comparing Treatment Groups. EphrinA1-Fc treated females and IgG females 1 day post-MI box plots for *m/z* 567.6, 617.7, 859.1 and 908.1

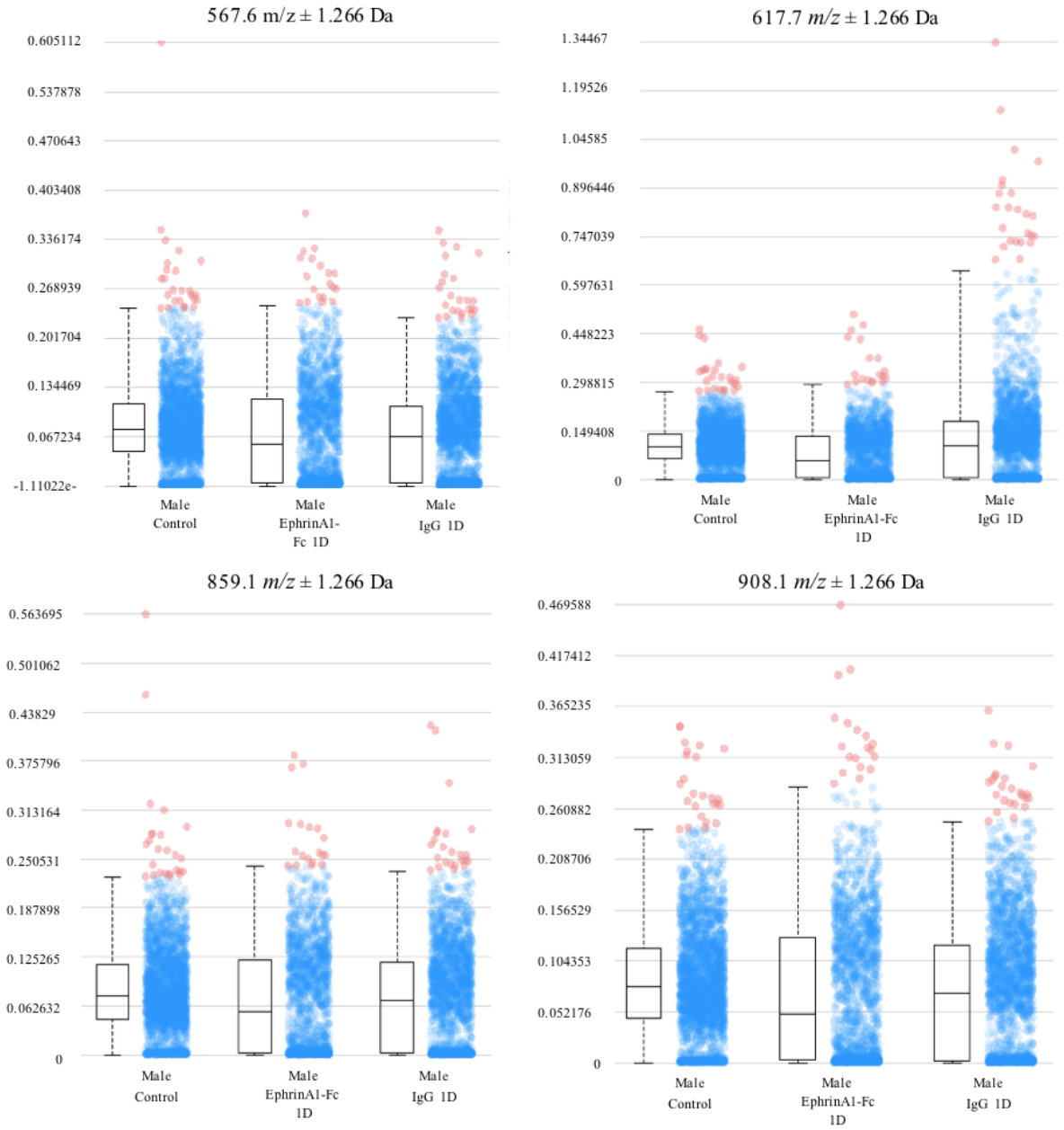

Figure 20. 1 Day Male EphrinA1 Expression Box Plots Treatment Groups. EphrinA1-Fc treated males and IgG males 1 day post-MI box plots for *m/z* 567.6, 617.7, 859.1, and 908.1

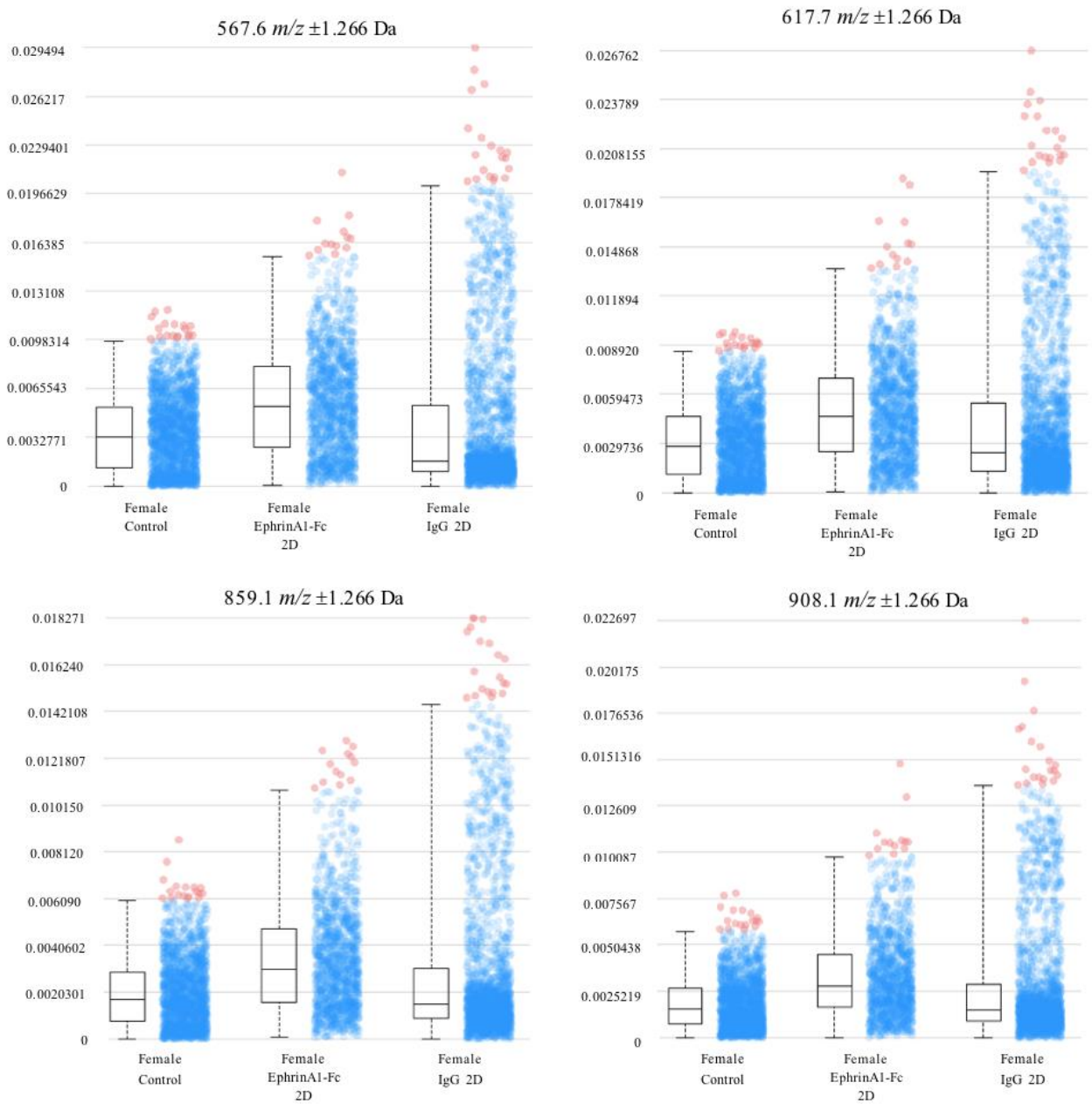

Figure 21. 2 Day Female EphrinA1 Expression Box Plots Treatment Groups. EphrinA1-Fc treated females and IgG males 2 days post-MI box plots for *m/z* 567.6, 617.7, 859.1, and 908.1

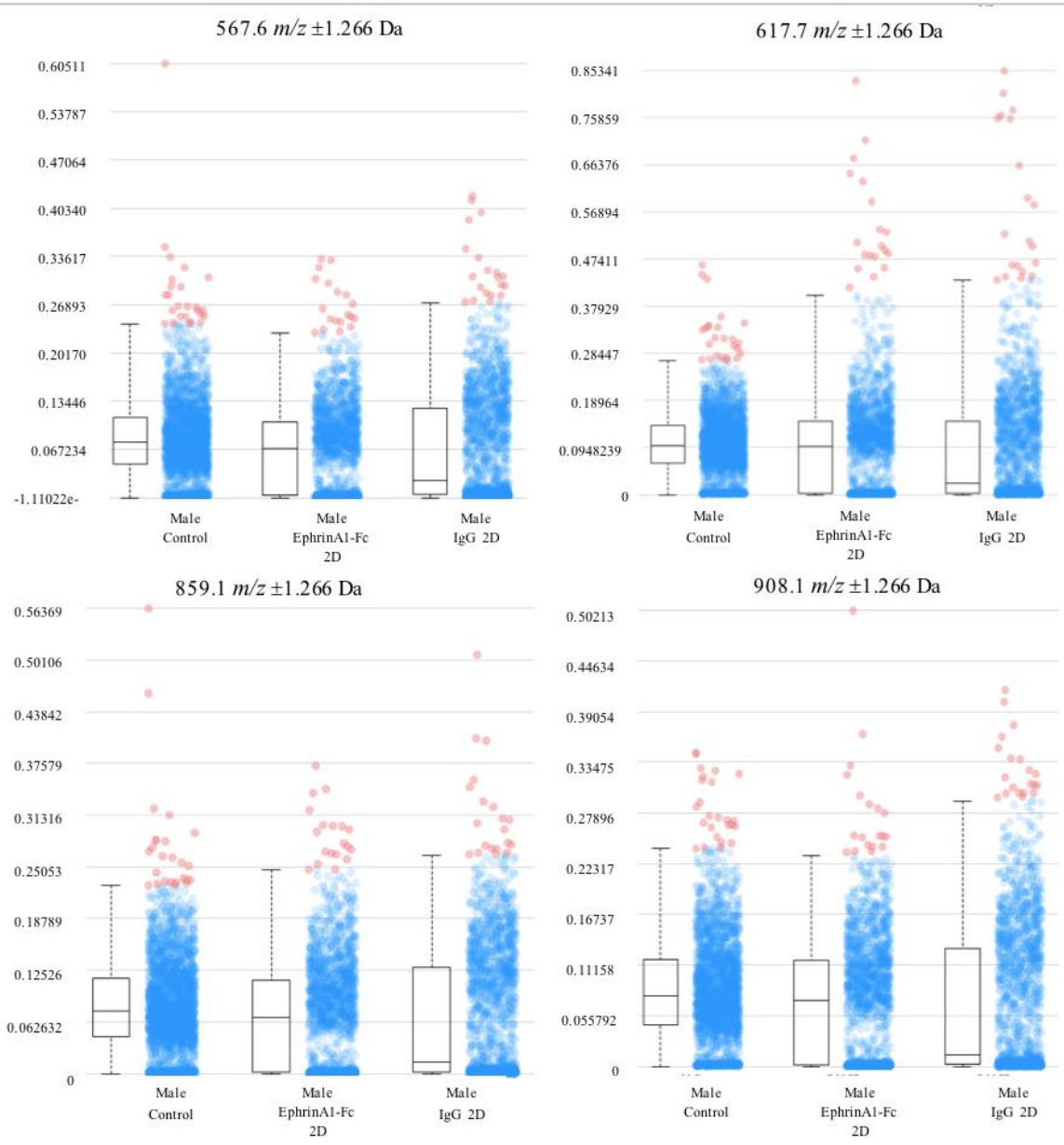

Figure 22. 2 Day Male EphrinA1 Expression Box Plots Treatment Groups. EphrinA1-Fc treated males and IgG males 2 days post-MI box plots for *m/z* 567.6, 617.7, 859.1, and 908.1

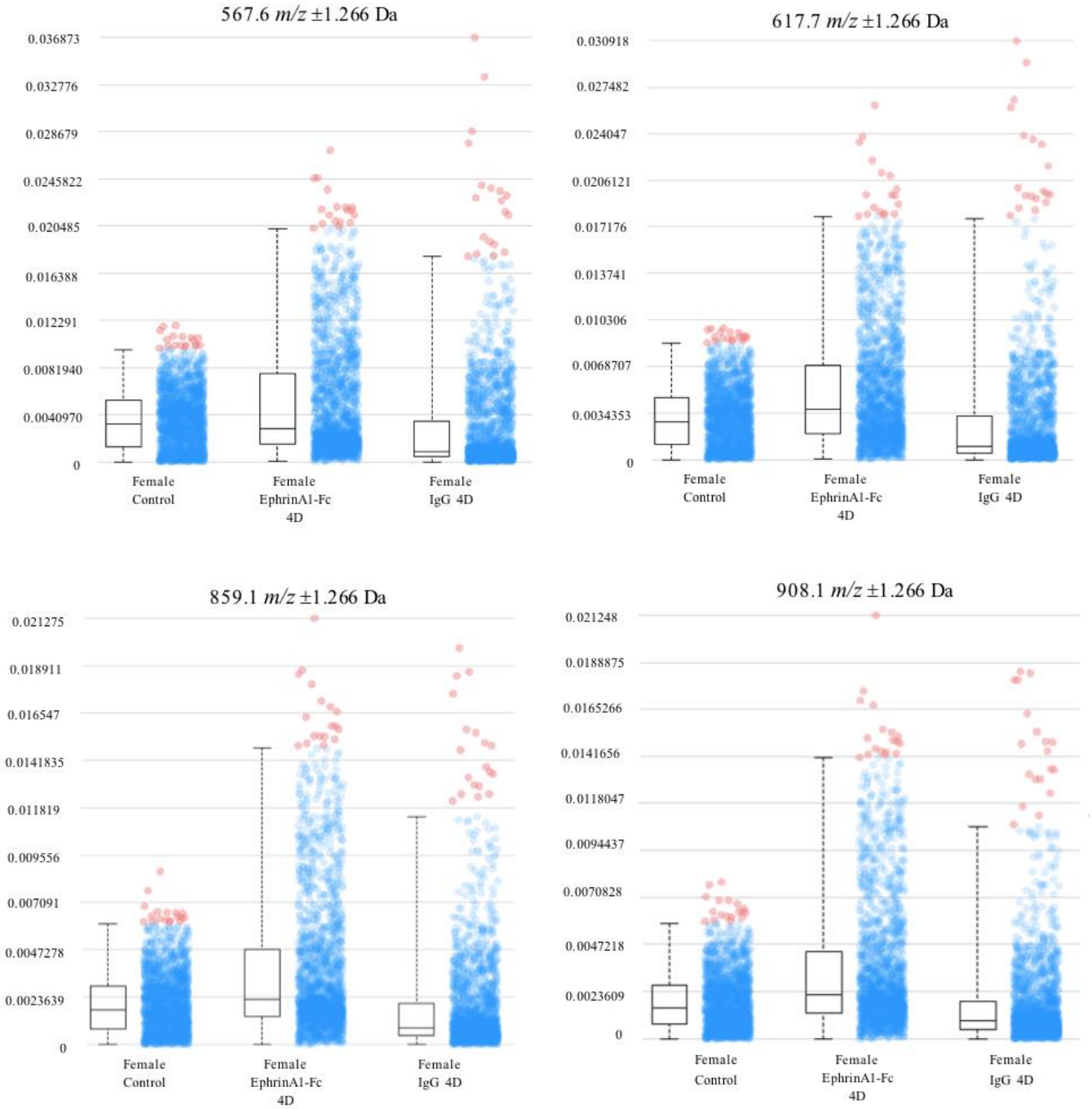

Figure 23. 4 Day Female EphrinA1 Expression Box Plots Treatment Groups. EphrinA1-Fc treated females and IgG males 4 days post-MI box plots for *m/z* 567.6, 617.7, 859.1, and 908.1

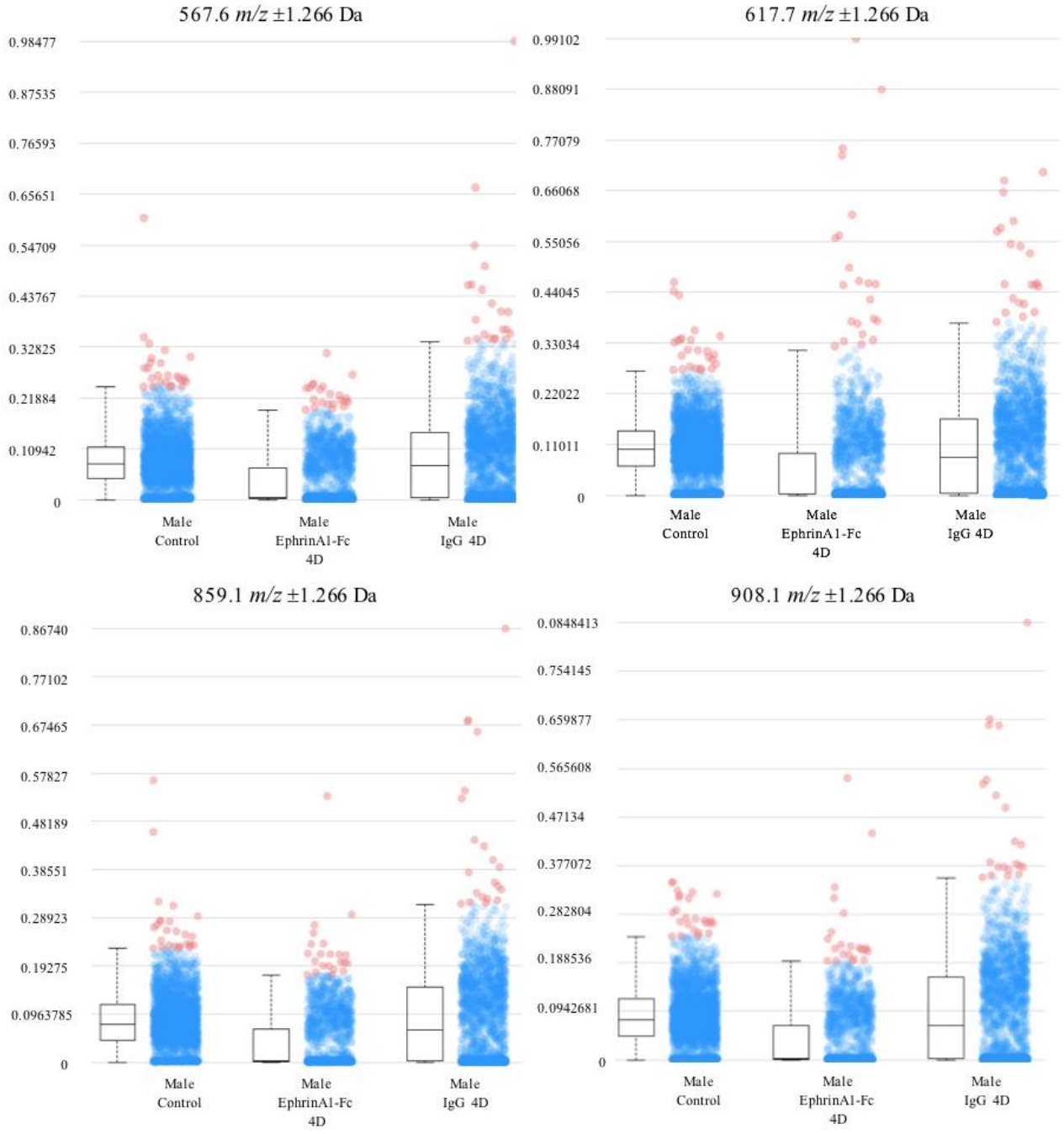

Figure 24. 4 Day Male EphrinA1 Expression Box Plots Treatment Groups. EphrinA1-Fc treated males and IgG males 4 days post-MI box plots for *m/z* 567.6, 617.7, 859.1, and 908.1

In contrast to the female data, male data do not follow the same trends. Post-MI males have a higher average mean intensity than the male non-injured controls for either the ephrinA1-Fc or the IgG treatment group. At 1-day post-MI it is demonstrated (Fig. 20) that average mean intensity is decreased for ephrinA1-Fc treated mice than the non-injured and IgG treated group. In addition, the depression of average mean intensity for the ephrinA1-Fc group the data suggest the IgG group has similar expression to that of the male control. Two days post-MI (Fig. 22) suggest that average mean intensities for endogenous ephrinA1 are higher than those of the IgG group however not as high as the non-injured control group. The 4-day post-MI data (Fig. 24) follow the same general responses as the 1-day time point with endogenous ephrinA1 average mean intensity being depressed as compared to the non-injured control and the IgG group, whereas the 7-day time point (Fig. 26) seems to be most similar to the 2-day time point with ephrinA1 treated animals having higher average mean intensities that IgG but lower than the non-injured control. Overall, when comparing male and female intensity plots, female time points 2, 4, and 7 days have higher expression of endogenous ephrinA1 than is seen in the non-injured control when treated with ephrinA1-Fc. The average mean intensities shown for the female ephrinA1-Fc group at those time points are as high as those seen in the male control non-injured tissue which as previously stated was found to be on average higher than female control. The mechanism of action for ephrinA1 as a potential therapeutic is currently unknown however, it is of vital importance to further investigate differences between sex in order to gain a deeper understanding of ephrinA1-Fc and the effects and influences it may have on cardiac tissue. In addition, it is necessary to understand the interactions between ephrinA1 and the EphA family receptors. To understand the interactions between ephrinA1 and EphARs, it is important to know the spatial distribution and relative levels

and then correlate these to changes in other signaling mediators temporally and spatially to shed light on possible mechanisms of action, optimization of timing and dose delivery, and cell-cell relationships that govern wound healing.

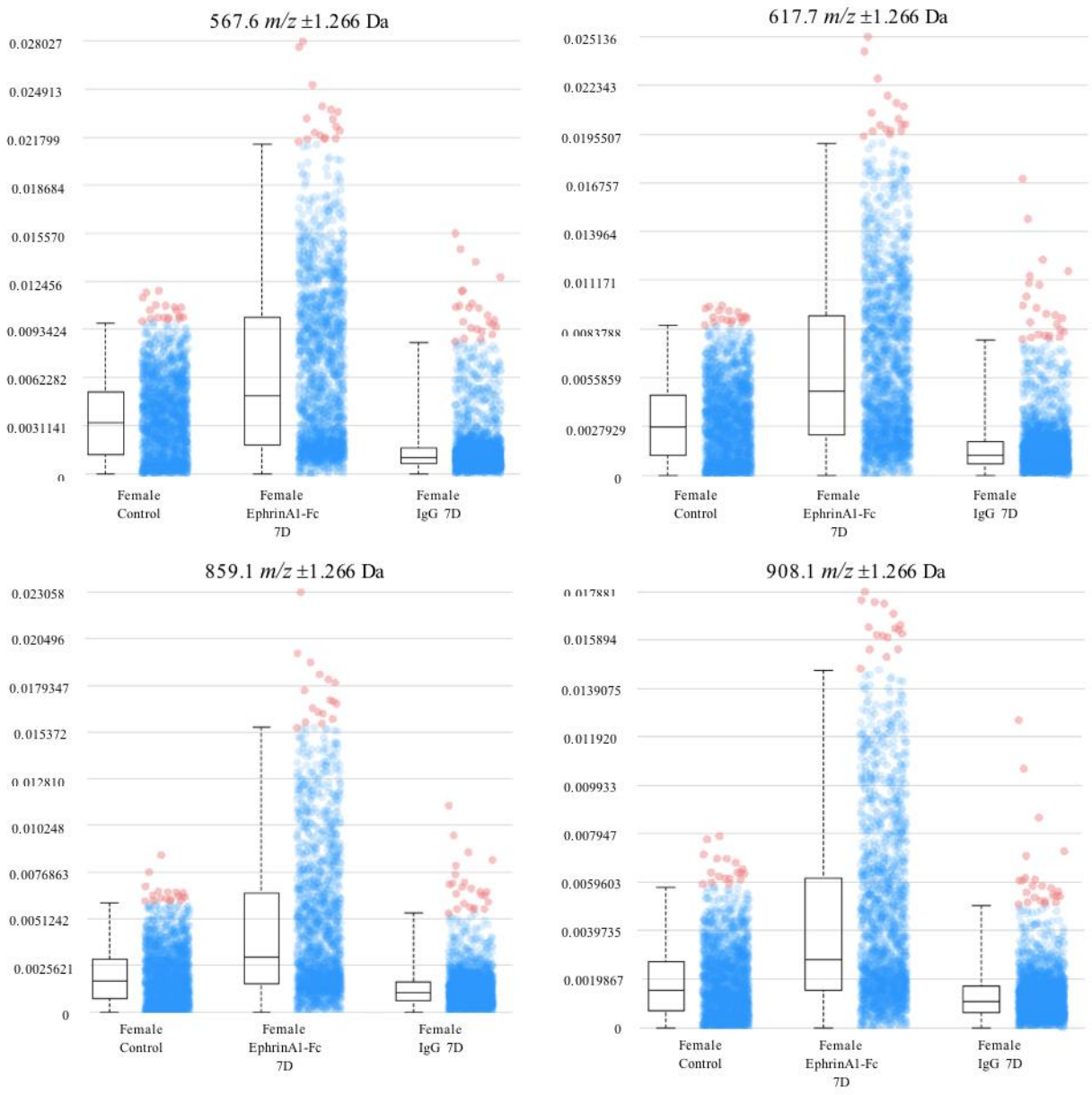

Figure 25. 7 Day Female EphrinA1 Expression Box Plots Treatment Groups.EphrinA1-Fc treated females and IgG males 7 days post- MI box plots for *m/z* 567.6, 617.7, 859.1, and 908.1

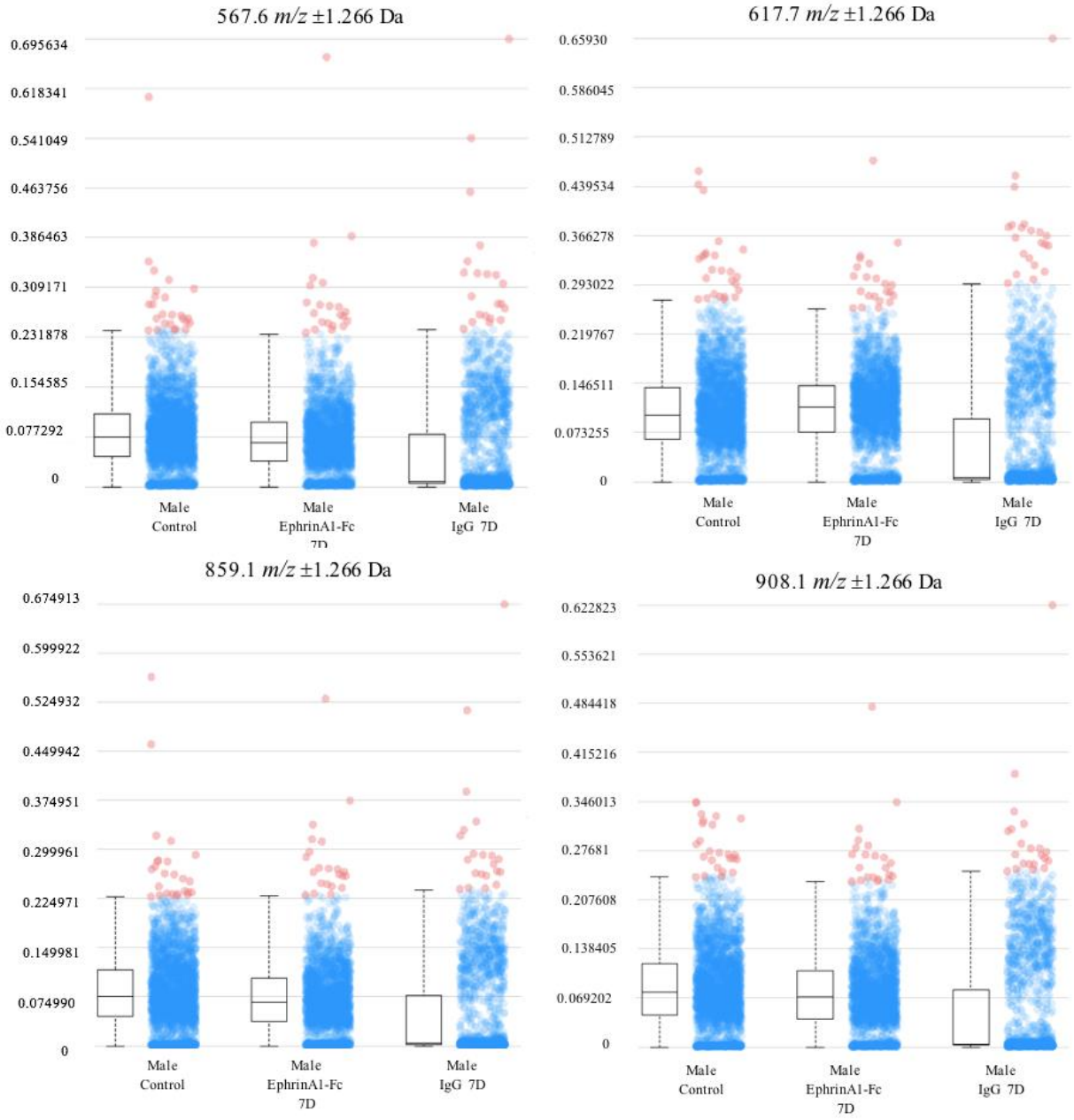

Figure 26. 7 Day Male EphrinA1 Expression Box Plots Treatment Groups. EphrinA1-Fc treated males and IgG males 7 days post-MI box plots for *m/z* 567.6, 617.7, 859.1, and 908.1

CHAPTER 6: CONCLUSION

Mice treated with ephrinA1-Fc at the time of coronary artery ligation in acute I/R and nonreperfused infarction show more favorable outcomes as compared to those who do not receive this treatment (Dries et al., 2011, DuSablon, 2017, O'Neal et al., 2013). After gaining an understanding of the spatial distribution of endogenous ephrinA1 in healthy non-injured tissue, we studied how it was affected by ischemia to determine how an exogenous treatment of ephrinA1-Fc effects the distribution and spatial location of endogenous ephrinA1 post-MI. First, the study of intact ephrinA1 in cardiac tissue from healthy, uninjured controls and from mice 4 days post-MI confirmed previous research conducted using IHC methods in showing a decrease in ephrinA1 expression in injured regions of the heart. In addition to confirming previous work MALDI-MSI provided spatial location and distribution of endogenous proteins in an alternative, and significantly more powerful method generating customized high-resolution images of ephrinA1. Due to the large size of intact ephrinA1 trypsin, enzymatic digestion was required to further examine ephrinA1 in cardiac tissue

Optimization of enzymatic digestion and matrix selection was necessary to best visualize endogenous ephrinA1. To best study the nature of the trypsin digestion ephrinA1-His tag standards were initially used alone on an ITO slide in order to evaluate the behavior of ephrinA1 when exposed to trypsin digestion and different matrices. Previous studies by our lab showed the use of SA and CHCA for MALDI-MSI on tissue for the identification of intact ephrinA1 (Lefcoski et al. 2018). Other matrices such as DHB or were not used due to them being more effective at detecting low molecular molecules. The use of ephrinA1-His tag standards revealed that SA matrix was the most effective matrix for the study of ephrinA1 after trypsin digestion. Another common matrix

CHCA was tested and compared to SA, but it was found to be less effective in detecting ephrinA1 peptides. Furthermore, the CHCA matrix was found to have a polymerization effect with the ephrinA1-His tag standard that was not seen while using SA.

In addition to this, trypsin concentration was varied, including concentrations of 100, 40, and 20 µg/mL and it was determined that 40µg/mL was optimal for adequate digestion of the ephrinA1-His tag standard with a digestion length of 4 hours at 37 °C.

Next, these optimized parameters for enzymatic digestion and matrix selection enzymatic digestion of endogenous ephrinA1 in cardiac tissue were used to continue the study of ephrinA1 in cardiac tissue. EphrinA1-His tag standards were used in conjunction with tissue sections in order to determine relative quantitation of endogenous ephrinA1 levels. The ephrinA1-His tag was added in multiple concentrations as a standard curve. Imaging the *m/z* intensities for peptide fragments that were known to be in endogenous ephrinA1 indicated that tissue sections were approximately 35 ng per section (sections averaged 9.425 mm^2). Up to this point, MSI for relative quantitation has been shown very little in literature and was the obvious necessary next step to advance this field.

Finally, the development of a relative quantitation using MALDI-MSI for endogenous ephrinA1 provided an opportunity to investigate further how ephrinA1-Fc affects the heart when used as therapeutic. Expression levels of endogenous ephrinA1 are shown to vary substantially with different treatments shown in Fig 20-27. In addition to this variation, it has been shown that differences in sex show different outcomes post-MI with women having higher mortality rates as compared to men (Vaccarino et al 1995, Jneid et al., 2008, Leifheit-Limson et al., 2015) , as well as different expression profiles of endogenous ephrinA1 at multiple time points post-MI. Although

these experiments regarding sex differences and post-MI time points have upcoming additional studies, this data provides vital insight that was previously unknown.

Overall, MALDI-MSI improved our understanding of the influence and effects of ephrinA1-Fc as a therapeutic for MI. More specifically, MALDI-MSI will aid in the determination of spatial location, distribution, and relative quantitation of the EphA-R will provide a valuable key in understanding the relationship between endogenous ephrinA1, its cognate receptors, and the downstream signaling pathways. Beyond this, we now have the capabilities to determine how the EphA-R respond in tissue post-MI with and without treatment of ephrinA1-Fc.

REFERENCE

Aichler, Michaela, and Axel Walch. 2015. “MALDI Imaging Mass Spectrometry: Current Frontiers and Perspectives in Pathology Research and Practice.” *Laboratory Investigation; a Journal of Technical Methods and Pathology* 95 (4): 422–31. https://doi.org/10.1038/labinvest.2014.156.

Albalat, Amaya, Angelique Stalmach, Vasiliki Bitsika, Justyna Siwy, Joost P. Schanstra, Alexandros D. Petropoulos, Antonia Vlahou, et al. 2013. “Improving Peptide Relative Quantification in MALDI-TOF MS for Biomarker Assessment.” *Proteomics* 13 (20): 2967–75. https://doi.org/10.1002/pmic.201300100.

Benjamin, Emelia J., Michael J. Blaha, Stephanie E. Chiuve, Mary Cushman, Sandeep R. Das, Rajat Deo, Sarah D. de Ferranti, et al. 2017. “Heart Disease and Stroke Statistics—2017 Update: A Report From the American Heart Association.” *Circulation*, January, CIR.0000000000000485. https://doi.org/10.1161/CIR.0000000000000485.

Brantley, Dana M., Nikki Cheng, Erin J. Thompson, Qing Lin, Rolf A. Brekken, Philip E. Thorpe, Rebecca S. Muraoka, et al. 2002. “Soluble Eph A Receptors Inhibit Tumor Angiogenesis and Progression in Vivo.” *Oncogene* 21 (46): 7011–26. https://doi.org/10.1038/sj.onc.1205679.

Bucknall, Martin, Kim Y. C. Fung, and Mark W. Duncan. 2002. “Practical Quantitative Biomedical Applications of MALDI-TOF Mass Spectrometry.” *Journal of the American Society for Mass Spectrometry* 13 (9): 1015–27. https://doi.org/10.1016/S1044-0305(02)00426-9.

Caprioli, R. M., T. B. Farmer, and J. Gile. 1997. “Molecular Imaging of Biological Samples: Localization of Peptides and Proteins Using MALDI-TOF MS.” *Analytical Chemistry* 69 (23): 4751–60.

Chen, Bijun, and Nikolaos G. Frangogiannis. 2017. “Immune Cells in Repair of the Infarcted Myocardium.” *Microcirculation (New York, N.Y.: 1994)* 24 (1). https://doi.org/10.1111/micc.12305.

Cheng, Nikki, Dana M. Brantley, and Jin Chen. 2002. “The Ephrins and Eph Receptors in Angiogenesis.” *Cytokine & Growth Factor Reviews* 13 (1): 75–85.

Chumbley, Chad W., Michelle L. Reyzer, Jamie L. Allen, Gwendolyn A. Marriner, Laura E. Via, Clifton E. Barry, and Richard M. Caprioli. 2016. “Absolute Quantitative MALDI Imaging Mass Spectrometry: A Case of Rifampicin in Liver Tissues.” *Analytical Chemistry* 88 (4): 2392–98. https://doi.org/10.1021/acs.analchem.5b04409.

Clemis, Elizabeth J., Derek S. Smith, Alexander G. Camenzind, Ryan M. Danell, Carol E. Parker, and Christoph H. Borchers. 2012. “Quantitation of Spatially-Localized Proteins in Tissue Samples Using MALDI-MRM Imaging.” *Analytical Chemistry* 84 (8): 3514–22. https://doi.org/nvestigating quantitation of phosphorylation using MALDI-TOF mass spectrometry.

Cornett, Dale S., Michelle L. Reyzer, Pierre Chaurand, and Richard M. Caprioli. 2007. “MALDI Imaging Mass Spectrometry: Molecular Snapshots of Biochemical Systems.” *Nature Methods* 4 (10): 828–33. https://doi.org/10.1038/nmeth1094.

Coulthard, Mark G., Michael Morgan, Trent M. Woodruff, Thiruma V. Arumugam, Stephen M. Taylor, Todd C. Carpenter, Martin Lackmann, and Andrew W. Boyd. 2012. “Eph/Ephrin Signaling in Injury and Inflammation.” *The American Journal of Pathology* 181 (5): 1493–1503. https://doi.org/10.1016/j.ajpath.2012.06.043.

Datta, Kaberi, Trayambak Basak, Swati Varshney, Shantanu Sengupta, and Sagartirtha Sarkar. 2017.

Quantitative Proteomic Changes during Post Myocardial Infarction Remodeling Reveals Altered Cardiac Metabolism and Desmin Aggregation in the Infarct Region." *Journal of Proteomics* 152: 283–99. https://doi.org/10.1016/j.jprot.2016.11.017.

Dixon, Jennifer A., and Francis G. Spinale. 2010. "Pathophysiology of Myocardial Injury and Remodeling: Implications for Molecular Imaging." *Journal of Nuclear Medicine: Official Publication, Society of Nuclear Medicine* 51 Suppl 1 (May): 102S-106S. https://doi.org/10.2967/jnumed.109.068213.

Dodelet, Vincent C., and Elena B. Pasquale. 2000. "Eph Receptors and Ephrin Ligands: Embryogenesis to Tumorigenesis." *Oncogene* 19 (49): 5614–19. https://doi.org/10.1038/sj.onc.1203856.

Dries, Jessica L, Susan D Kent, and Jitka A I Virag. 2011. "Intramyocardial Administration of Chimeric EphrinA1-Fc Promotes Tissue Salvage Following Myocardial Infarction in Mice." *The Journal of Physiology* 589 (Pt 7): 1725–40. https://doi.org/10.1113/jphysiol.2010.202366.

DuSablon, A.; Parks, J.; Whitehurst, K.; Estes, H.; Chase, R.; Vlahos, E.; Sharma, U.; Wert, D.; Virag, J. 2017. "EphrinA1-Fc Attenuates Myocardial Ischemia/Reperfusion Injury in Mice." *PLoS One* 12 (12): e0189307. https://doi.org/10.1371/journal.pone.0189307.

DuSablon, Augustin, Susan Kent, Anita Coburn, and Jitka Virag. 2014. "EphA2-Receptor Deficiency Exacerbates Myocardial Infarction and Reduces Survival in Hyperglycemic Mice." *Cardiovascular Diabetology* 13 (August): 114. https://doi.org/10.1186/s12933- 014-0114-y.

Easty, D. J., S. P. Hill, M. Y. Hsu, M. E. Fallowfield, V. A. Florenes, M. Herlyn, and D. C. Bennett. 1999. "Up-Regulation of EphrinA1 during Melanoma Progression." *International Journal of Cancer* 84 (5): 494–501.

Goichberg, Polina, Yingnan Bai, Domenico D'Amario, João Ferreira-Martins, Claudia Fiorini, Hanqiao Zheng, Sergio Signore, et al. 2011. "The Ephrin A1-EphA2 System Promotes Cardiac Stem Cell Migration after Infarction." *Circulation Research* 108 (9): 1071–83. https://doi.org/10.1161/CIRCRESAHA.110.239459.

Guo, Yichen, Lianqun Cui, Shiliang Jiang, Airong Zhang, and Shu Jiang. 2017. "Proteomics of Acute Heart Failure in a Rat Post-Myocardial Infarction Model." *Molecular Medicine Reports* 16 (2): 1946–56. https://doi.org/10.3892/mmr.2017.6820.

Himanen, Juha P., Laila Yermekbayeva, Peter W. Janes, John R. Walker, Kai Xu, Lakmali Atapattu, Kanagalaghatta R. Rajashankar, et al. 2010. "Architecture of Eph Receptor Clusters." *Proceedings of the National Academy of Sciences of the United States of America* 107 (24): 10860–65. https://doi.org/10.1073/pnas.1004148107.

Jneid, H., Fonarow, G.C., Cannon, C.P., Hernandez, A.F., Palacios, I.F., Maree, A.O., Wells, Q., Bozkurt, B., LaBresh, K.A., Liang, L., et al. (2008). Sex Differences in Medical Care and Early Death After Acute Myocardial Infarction. Circulation 118, 2803–2810.

Jones, Steven P., Xian-Liang Tang, Yiru Guo, Charles Steenbergen, David J. Lefer, Rakesh C. Kukreja, Maiying Kong, et al. 2015. "The NHLBI-Sponsored Consortium for PreclinicAl AssESsment of CARdioprotective Therapies (CAESAR): A New Paradigm for Rigorous, Accurate, and Reproducible Evaluation of Putative Infarct-Sparing Interventions in Mice, Rabbits, and Pigs." *Circulation Research* 116 (4): 572–86. https://doi.org/10.1161/CIRCRESAHA.116.305462.

Knochenmuss, Richard, Volker Karbach, Ursula Wiesli, Kathrin Breuker, and Renato Zenobi. 1998. The Matrix Suppression Effect in Matrix-Assisted Laser Desorption/Ionization: Application to Negative Ions and Further Characteristics." *Rapid Communications in Mass*

Spectrometry 12 (9): 529–34. https://doi.org/MALDI-TOF mass spectrometry of a combinatorial peptide library: effect of matrix composition on signal suppression.

Leifheit-Limson, E.C., D'Onofrio, G., Daneshvar, M., Geda, M., Bueno, H., Spertus, J.A., Krumholz, H.M., and Lichtman, J.H. (2015). Sex Differences in Cardiac Risk Factors, Perceived Risk, and Health Care Provider Discussion of Risk and Risk Modification Among Young Patients With Acute Myocardial Infarction: The VIRGO Study. Journal of the American College of Cardiology 66, 1949–1957.

Lefcoski, Stephan, Kimberly Kew, Shaun Reece, Maria J. Torres, Justin Parks, Sky Reece, Lisandra E. de Castro Brás, and Jitka A. I. Virag. 2018. "Anatomical-Molecular Distribution of EphrinA1 in Infarcted Mouse Heart Using MALDI Mass Spectrometry Imaging." *Journal of the American Society for Mass Spectrometry*, January. https://doi.org/10.1007/s13361-017-1869-7.

Lema Tomé, Carla M., Enzo Palma, Sara Ferluga, W. Todd Lowther, Roy Hantgan, Jill Wykosky, and Waldemar Debinski. 2012. "Structural and Functional Characterization of Monomeric EphrinA1 Binding Site to EphA2 Receptor." *The Journal of Biological Chemistry* 287 (17): 14012–22. https://doi.org/10.1074/jbc.M111.311670.

Liu, Zhaoyang, and Kevin L. Schey. 2005. "Optimization of a MALDI TOF-TOF Mass Spectrometer for Intact Protein Analysis." *Journal of the American Society for Mass Spectrometry* 16 (4): 482–90. https://doi.org/10.1016/j.jasms.2004.12.018.

Ma, Yonggang, Andriy Yabluchanskiy, and Merry L. Lindsey. 2013. "Neutrophil Roles in Left Ventricular Remodeling Following Myocardial Infarction." *Fibrogenesis & Tissue Repair* 6 (1): 11. https://doi.org/10.1186/1755-1536-6-11.

Menger, Robert F., Whitney L. Stutts, Dhanalakshmi S. Anbukumar, John A. Bowden, David A. Ford,

and Richard A. Yost. 2012. “MALDI Mass Spectrometric Imaging of Cardiac Tissue Following Myocardial Infarction in a Rat Coronary Artery Ligation Model.” *Analytical Chemistry* 84 (2): 1117–25. https://doi.org/10.1021/ac202779h.

Michael, L. H., C. M. Ballantyne, J. P. Zachariah, K. E. Gould, J. S. Pocius, G. E. Taffet, C. J. Hartley, et al. 1999. “Myocardial Infarction and Remodeling in Mice: Effect of Reperfusion.” *The American Journal of Physiology* 277 (2 Pt 2): H660-668.

Mobley, J. (2008). General Trypsin Digestion Using Urea Protocol for Cell Lysates; LCMS on LTQ. [online] UAB Mass Spectrometry/Proteomics. Available at:https://www.uab.edu/medicine/msproteomics/images/eduProtPDF/cellstrypsin.pdf [Accessed 2 Oct. 2017]

Mosca, L., Barrett-Connor, E., and Wenger, N.K. (2011). Sex/Gender Differences in Cardiovascular Disease Prevention: What a Difference a Decade Makes. Circulation *124*, 2145–2154.

Nicklay, Joshua J., Glenn A. Harris, Kevin L. Schey, and Richard M. Caprioli. 2013. “MALDI Imaging and in Situ Identification of Integral Membrane Proteins from Rat Brain Tissue Sections.” *Analytical Chemistry* 85 (15): 7191–96. https://doi.org/10.1021/ac400902h.

O’Neal, Wesley T., William F. Griffin, Jessica L. Dries-Devlin, Susan D. Kent, Jin Chen, Monte S. Willis, and Jitka A. I. Virag. 2013. “Ephrin-Eph Signaling as a Potential Therapeutic Target for the Treatment of Myocardial Infarction.” *Medical Hypotheses* 80 (6): 738–44. https://doi.org/10.1016/j.mehy.2013.02.024.

O’Neal, Wesley T., William F. Griffin, Susan D. Kent, Filza Faiz, Jonathan Hodges, Jackson Vuncannon, and Jitka A. I. Virag. 2014. “Deletion of the EphA2 Receptor Exacerbates

Myocardial Injury and the Progression of Ischemic Cardiomyopathy." *Frontiers in Physiology* 5132. https://doi.org/10.3389/fphys.2014.00132.

Pandey, A., H. Shao, R. M. Marks, P. J. Polverini, and V. M. Dixit. 1995. "Role of B61, the Ligand for the Eck Receptor Tyrosine Kinase, in TNF-Alpha-Induced Angiogenesis." *Science (New York, N.Y.)* 268 (5210): 567–69.

Pasquale, Elena B. 2008. "Eph-Ephrin Bidirectional Signaling in Physiology and Disease." *Cell* 133 (1): 38–52. https://doi.org/10.1016/j.cell.2008.03.011.

Reich, Richard F., Kasia Cudzilo, Joseph A. Levisky, and Richard A. Yost. 2010. "Quantitative MALDI-MS(n) Analysis of Cocaine in the Autopsied Brain of a Human Cocaine User Employing a Wide Isolation Window and Internal Standards." *Journal of the American Society for Mass Spectrometry* 21 (4): 564–71. https://doi.org/10.1016/j.jasms.2009.12.014.

Reimer, K. A., and R. B. Jennings. 1979. "The 'Wavefront Phenomenon' of Myocardial Ischemic Cell Death. II. Transmural Progression of Necrosis within the Framework of Ischemic Bed Size (Myocardium at Risk) and Collateral Flow." *Laboratory Investigation; a Journal of Technical Methods and Pathology* 40 (6): 633–44.

Schlosser, Gitta, Gabriella Pocsfalvi, Emőke Huszár, Antonio Malorni, and Ferenc Hudecz. 2005. "MALDI-TOF Mass Spectrometry of a Combinatorial Peptide Library: Effect of Matrix Composition on Signal Suppression." *Journal of Mass Spectrometry* 40 (12): 1590–94. https://doi.org/10.1002/jms.937.

Seeley, Erin H., Kristina Schwamborn, and Richard M. Caprioli. 2011. "Imaging of Intact Tissue Sections: Moving beyond the Microscope." *Journal of Biological Chemistry* 286 (29): 25459–

66. https://doi.org/10.1074/jbc.R111.225854.

Sun, Na, Yin Wu, Kazutaka Nanba, Silviu Sbiera, Stefan Kircher, Thomas Kunzke, Michaela Aichler, et al. 2018. “High-Resolution Tissue Mass Spectrometry Imaging Reveals a Refined Functional Anatomy of the Human Adult Adrenal Gland.” *Endocrinology* 159 (3): 1511–24. https://doi.org/10.1210/en.2018-00064.

Surawska, H., P. C. Ma, and R. Salgia. 2004. “The Role of Ephrins and Eph Receptors in Cancer.” *Cytokine & Growth Factor Reviews* 15 (6): 419–33. https://doi.org/10.1016/j.cytogfr.2004.09.002.

Szájli, Emília, Tamás Fehér, and Katalin F. Medzihradszky. 2008. “Investigating the Quantitative Nature of MALDI-TOF MS.” *Molecular & Cellular Proteomics* 7 (12): 2410–18. https://doi.org/10.1074/mcp.M800108-MCP200.

Teklezgi, Belin G., Annapurna Pamreddy, Sooraj Baijnath, Hendrik G. Kruger, Tricia Naicker, Nirmala D. Gopal, and Thavendran Govender. 2018. “Time-Dependent Regional Brain Distribution of Methadone and Naltrexone in the Treatment of Opioid Addiction.” *Addiction Biology*, February. https://doi.org/10.1111/adb.12609.

Vaccarino, Viola, Krumholz M. Harlan, Berkman F. Lisa, Horwitz I. Ralph. 1995. “Sex Differences in Mortality After Myocardial Infarction Is There Evidence for an Increased Risk for Women?” *Circulation,* March. https://doi.org/10.1161/01.CIR.91.6.1861.

Vandervelde, Susanne, Machteld J. van Amerongen, Rene A. Tio, Arjen H. Petersen, Marja J. A. van Luyn, and Martin C. Harmsen. 2006. “Increased Inflammatory Response and Neovascularization in Reperfused vs. Non-Reperfused Murine Myocardial Infarction.” *Cardiovascular Pathology: The Official Journal of the Society for Cardiovascular Pathology* 15 (2): 83–90.

https://doi.org/10.1016/j.carpath.2005.10.006.

Wagner, Craig D., John T. Hall, Wendy L. White, Luke A. D. Miller, and Jon D. Williams. 2007. "Automated Mass Correction and Data Interpretation for Protein Open-Access Liquid Chromatography-Mass Spectrometry." *Journal of Mass Spectrometry: JMS* 42 (2): 139– 49. https://doi.org/10.1002/jms.1174.

Wang, Xin, Yaowu Sha, and Runtao Li. 2004. "Fragmentation Patterns of Novel Dispirocyclopiperazinium Dibromides with Strong Analgesic Activity under Electrospray Ionization Tandem Mass Spectrometry Conditions." *Rapid Communications in Mass Spectrometry* 18 (8): 829–33. https://doi.org/10.1002/rcm.1407.

Xu, Qian, Wan-Chen Lin, Rebecca S. Petit, and Jay T. Groves. 2011. "EphA2 Receptor Activation by Monomeric EphrinA1 on Supported Membranes." *Biophysical Journal* 101 (11): 2731–39. https://doi.org/10.1016/j.bpj.2011.10.039.

Yang XP, Liu YH, Rhaleb NE, Kurihara N, Kim HE, Carretero OA. Echocardiographic assessment of cardiac function in conscious and anesthetized mice. Am J Physiol. 1999;277(5 Pt 2):H1967–74. Epub 1999/11/24.

Yang, Junhai, and Richard M. Caprioli. 2011. "Matrix Sublimation/Recrystallization for Imaging Proteins by Mass Spectrometry at High Spatial Resolution." *Analytical Chemistry* 83 (14): 5728–34. https://doi.org/10.1021/ac200998a.

Zhang, Yaoyang, Bryan R. Fonslow, Bing Shan, Moon-Chang Baek, and John R. Yates. 2013. "Protein Analysis by Shotgun/Bottom-up Proteomics." *Chemical Reviews* 113 (4): 2343– 94. https://doi.org/10.1021/cr3003533.

APPENDEX A

East Carolina University
Tomorrow starts here.

Animal Care and
Use Committee
212 Ed Warren Life
Sciences Building
East Carolina University
Greenville, NC 27834-4354

252-744-2436 office
252-744-2355 fax

March 20, 2018

Jitka Virag, Ph.D.
Department of Physiology
EW Life Sciences Building
East Carolina University

Dear Dr. Virag:

Your Animal Use Protocol entitled, "Murine Model of Myocardial Infarct Repair" (AUP #Q228d) was reviewed by this institution's Animal Care and Use Committee on March 20, 2018. The following action was taken by the Committee:

"Approved as submitted"

Please contact Aaron Hinkle at 744-2997 prior to hazard use

A copy is enclosed for your laboratory files. Please be reminded that all animal procedures must be conducted as described in the approved Animal Use Protocol. Modifications of these procedures cannot be performed without prior approval of the ACUC. The Animal Welfare Act and Public Health Service Guidelines require the ACUC to suspend activities not in accordance with approved procedures and report such activities to the responsible University Official (Vice Chancellor for Health Sciences or Vice Chancellor for Academic Affairs) and appropriate federal Agencies. **Please ensure that all personnel associated with this protocol have access to this approved copy of the AUP and are familiar with its contents.**

Sincerely yours,

Susan McRae, Ph.D.
Chair, Animal Care and Use Committee

SM/jd

Enclosure

EAST CAROLINA UNIVERSITY
ANIMAL USE PROTOCOL (AUP) FORM
LATEST REVISION APRIL, 2017

Project Title:

Murine Model of Myocardial Infarct Repair

	Principal Investigator	Secondary Contact
Name	Jitka Virag	Click here to enter text.
Dept.	Physiology	Click here to enter text.
Office Ph #	744-2777	Click here to enter text.
Cell Ph #	412-8216	Click here to enter text.
Pager #	Click here to enter text.	Click here to enter text.
Home Ph #	Click here to enter text.	Click here to enter text.
Email	viragj@ecu.edu	Click here to enter text.

For IACUC Use Only

AUP # P2280			
New/Renewal Renewal 3/7/18			
Full Review/Date	DR/Date		
Approval Date 3/20/18			
Study Type myocardial infarct model			
Pain/Distress Category D			
Surgery ✓	Survival ✓	Multiple	LSB 246 - myocardial infarction + mini-pumps implantation
Prolonged Restraint			
Food/Fluid Regulation			
Other			
Hazard Approval/Dates	Rad	IBC 3/19/18	EHS marcaine,
OHP Enrollment		ephrin A1-Fc,	pentobarbital,
Mandatory Training			isoflurane,
Amendments Approved		IgG-Fc,	tribromoethanol,
		transgenic	rapamycin,

bafilomycin, bromodeoxyuridine, heparin, AKT inhibitor, 3-Methyladenine, ketamine/xylazine

I. Personnel

A. Principal Investigator(s):

Jitka Virag

B. Department(s):

Physiology

C. List all personnel (PI's, co-investigators, technicians, students) that will be working with live animals and describe their qualifications and experience with these specific procedures. If people are to be trained, indicate by whom:

Name/Degree/Certification	Position/Role(s)/ Responsibilities in this Project	Required Online IACUC Training (Yes/No)	Relevant Animal Experience/Training (include species, procedures, number of years, etc.)
Jitka Virag, PhD	PI: design experiments and oversee study execution, perform surgeries	yes	21 years of rodent handling, 16 years of microsurgery, post-operative monitoring, and tissue collection
Robert Lust, PhD	Co-I: help train others microsurgical techniques and assist with studies	Yes	25+ years of small and large animal surgery
Lisandra de Castro Bras,PhD	Co-I: help train others microsurgical techniques and assist with studies	Yes	5+ years of animal handling and microsurgery
Justin Parks	Graduate student, will assist with animal preparation, post-operative observation, and tissue collection	Yes	Animal handling and tissue collection
Sam Vance	Graduate student, will assist with animal preparation, post-operative observation, and tissue collection	Yes	Animal handling, genotyping, colony maintenance, tissue collection
Click here to enter text.	Click here to enter text.	Choose an item.	Click here to enter text.
Click here to enter text.	Click here to enter text.	Choose an item.	Click here to enter text.
Click here to enter text.	Click here to enter text.	Choose an item.	Click here to enter text.
Click here to enter text.	Click here to enter text.	Choose an item.	Click here to enter text.
Click here to enter text.	Click here to enter text.	Choose an item.	Click here to enter text.